The hydrogen isotope signatures of autotrophy versus heterotrophy recorded in archaeal tetraether lipids

Authors: Jeemin H. Rhim[1,*], Sebastian Kopf[2], Jamie McFarlin[2,3], Harpreet Batther[2], Carolynn M. Harris[1], Alice Zhou[1], Xiahong Feng[1], Yuki Weber[5], Shelley Hoeft-McCann[5], Ann Pearson[5], and William D. Leavitt[1,6]

[1] Department of Earth Sciences, Dartmouth College
[2] Department of Geological Sciences, University of Colorado Boulder
[3] Department of Geology & Geophysics, University of Wyoming
[4] Department of Earth & Planetary Sciences, University of Michigan
[5] Department of Earth & Planetary Sciences, Harvard University
[6] Department of Chemistry, Dartmouth College

* Corresponding author: jrhim@ucsb.edu

^Current address: Jeemin H. Rhim, Department of Ecology, Evolution, and Marine Biology, University of California Santa Barbara, Santa Barbara, CA, USA; TBD.

Keywords: Archaeal lipids, tetraether lipids, GDGTs, biphytanes, hydrogen isotope, biomarkers

Abstract

The stable hydrogen isotope composition of archaeal lipids is emerging as a potential paleoenvironmental proxy, adding to the well-established application of plant leaf wax-derived *n*-alkanes in paleohydrological reconstruction. A handful of studies reported relatively invariant and depleted hydrogen isotope compositions for archaeal lipids despite the range of different organisms and growth conditions explored. However, how modes of metabolism affect the hydrogen isotope signatures of archaeal lipids remains poorly understood, limiting our ability to interpret archaeal lipid biomarker records from the environment. Here we conducted water isotope label experiments with a metabolically flexible and well-studied model archaeon *Archaeoglobus fulgidus* and quantified the hydrogen isotope fractionation between lipids and water in response to different carbon substrates and electron donor-acceptor pairs. The $^{2}H/^{1}H$ fractionation between lipids and water ($\varepsilon_{L/W}$) was overall negative, ranging from –280 to –226 ‰, and overlapped with the ranges observed for other archaea in previous studies. Isotope flux-balance model results suggest that ≥80 % and ≥50 % of lipid-bound H in *A. fulgidus* cultures originate from water during autotrophy and heterotrophy, respectively. The model results also suggest the final saturation during isoprenoid lipid biosynthesis catalyzed by a flavoenzyme geranylgeranyl reductase (GGR) likely contributes to the large $^{2}H/^{1}H$ fractionation observed in this study, consistent with isotope flux-balance model results for a different archaeon. Finally, we synthesized available data to compare $\varepsilon_{L/W}$ patterns across all three domains of life: Bacteria, Archaea and Eukarya. Emerging patterns between archaeal and eukaryotic lipids are consistent with the notion of highly

fractionating GGR, and the patterns between archaeal and bacterial lipids suggest that the general state of energy limitation may also contribute to depleted $\varepsilon_{L/W}$ observed in prokaryotic lipids. Altogether, these findings lend further support for the potential of archaeal lipid $\varepsilon_{L/W}$ as a paleohydrological proxy and provide a broader insight into the $^2H/^1H$ fractionation mechanisms potentially shared among prokaryotic and eukaryotic lipid biomarkers.

1. Introduction

Hydrogen (H) plays a crucial role in most metabolic processes and is incorporated into biological molecules, often with distinct isotope fractionation patterns. Consequently, the ratio of stable hydrogen isotopes ($^2H/^1H$) of certain biomolecules can be used to track the H isotope compositions of source water, or the operation of specific biosynthetic pathways (Estep and Hoering, 1980; Sessions et al., 1999; Hayes, 2001). Lipid-bound H in hydrocarbons may resist isotope exchange over geologic time scales for up to 10^4 to 10^8 years (Sessions et al., 2004). Thus, sedimentary record of lipid δ^2H can be applied to reconstruct past ecological or hydrological states (Sachse et al., 2012; Sessions, 2016; McFarlin et al., 2019). The δ^2H of lipids produced by photoautotrophic eukaryotes as well as chemoautotrophic and heterotrophic bacteria have been studied in detail for this reason (e.g., Sessions et al., 1999; Chikaraishi and Naraoka, 2003; Zhang and Sachs, 2007; Zhang et al., 2009; Sachse et al., 2012; Sachs, 2014; Dawson et al., 2015; Osburn et al., 2016; Leavitt et al., 2016; Wijker et al., 2019; McFarlin et al., 2019). The H isotope data on lipids produced by archaea, in contrast, are limited to only a handful of studies (e.g., Kaneko et al., 2011; Dirghangi and Pagani, 2013; Wu et al., 2020; Lengger et al., 2021; Leavitt et al., 2023). As a result, factors controlling the H isotope fractionation between lipid and water ($\varepsilon_{L/W}$) as well as the extent and limits of proxy applications are relatively well understood for eukaryotic and bacterial lipids, yet remain poorly understood for archaeal lipids.

The $\varepsilon_{L/W}$ values reflect a combination of source water δ^2H and the kinetic isotope effect (KIE) of enzymes involved in lipid biosynthesis. For lipids produced by photoautotrophic eukaryotes (e.g., plants and algae), KIE is relatively invariant but can be altered by some environmental factors (e.g., temperature, salinity, irradiance) and some factors intrinsic to an organism (e.g. growth rate in response to different stimuli and underlying genetics) (Sachs, 2014; Van Der Meer et al., 2015; Sachs and Kawka, 2015; Sachs et al., 2016, 2017; Maloney et al., 2016; Ladd and Sachs, 2017; Wolfshorndl et al., 2019; Bender, n.d.). In general, these are well studied in eukaryotes, and have been accounted for in hydroclimate proxy studies (Sachse et al., 2012; Sessions, 2016; McFarlin et al., 2019).

Bacterial lipids show significantly more range in $\varepsilon_{L/W}$ than eukaryotic lipids. Depending on the central metabolism a given bacteria operates, $\varepsilon_{L/W}$ can range from –400 to –200 ‰ (exclusively negative values) for (an)aerobic chemoautotrophs to –154 to +380 ‰, associated with aerobic heterotrophs (Sessions et al., 2002; Campbell et al., 2009; Zhang et al., 2009; Dawson et al., 2015; Osburn et al., 2016; Leavitt et al., 2016; Wijker et al., 2019). For lipids produced by aerobic

heterotrophs, H fluxes through $NADP^+$-reducing and NADPH-balancing reactions provide a quantitative explanation for the full range of $\varepsilon_{L/W}$ values observed (Wijker et al., 2019). Bacterial lipids found in sediments, especially those produced by aerobic heterotrophs, may have more useful applications as a proxies for microbial metabolism and ecology rather than past hydroclimate (Zhang et al., 2009; Wijker et al., 2019).

Less is known about the type(s) of information archaeal lipids record. Studies to-date indicate that archaeal lipids are generally depleted in ^2H, with $\varepsilon_{L/W}$ values comparable to those observed in eukaryotic photoautotrophs and bacterial chemoautotrophs (Kaneko et al., 2011; Dirghangi and Pagani, 2013; Wu et al., 2020; Lengger et al., 2021; Leavitt et al., 2023). In one recent study, continuous cultures of the obligate autotroph *Nitrosopumilus maritimus* revealed that $\varepsilon_{L/W}$ remains nearly constant across a 3-fold range in growth rate (Leavitt et al., 2023). Other studies have reported similarly negative $\varepsilon_{L/W}$ values for archaea grown under heterotrophic conditions (Kaneko et al., 2011; Dirghangi and Pagani, 2013; Wu et al., 2020; Lengger et al., 2021). However, it remains to be determined whether and how carbon metabolism affects $\varepsilon_{L/W}$ within a single organism. Testing this is important, considering that mixotrophy (using both autotrophic and heterotrophic carbon sources) is a widespread mode of metabolism in nature and that many archaea are adapted to fluctuating environments. For bacterial lipids, changes in carbon metabolism resulted in significantly different $\varepsilon_{L/W}$ values within a single organism for some species (e.g., *Cupriavidus oxalaticus* and *Paracoccus denitrificans*; Zhang et al., 2009; Osburn et al., 2016), but not in other species (sulfate-reducing bacteria; Dawson et al., 2015; Osburn et al., 2016; Leavitt et al., 2016). As such, understanding the role of carbon metabolism in setting archaeal lipid-H isotope compositions is important for interpreting archaeal lipids record from the environment. Furthermore, our current understanding of broader patterns of $\varepsilon_{L/W}$ that emerge from comparison across lipids produced by all three domains of life—Archaea, Bacteria, and Eukarya—is limited, despite the similarities observed among certain subgroups of different domains.

In this study, we first conducted pure culture experiments to better understand factors influencing $\varepsilon_{L/W}$ in archaeal lipids. A metabolically flexible model archaeon *Archaeoglobus fulgidus* was grown in batch cultures on different carbon substrates and electron donor-acceptor pairs (lactate-thiosulfate, lactate-sulfate, and H_2/CO_2-thiosulfate) to test the effect of metabolism on $\varepsilon_{L/W}$ within a single organism. All conditions included replicates with different water isotope compositions to track the fraction of water that gets incorporated into the final product lipid. The effect of growth phase was also assessed by comparing biomass harvested at exponential and stationary growth phases. We interpret the regression parameters derived from the water isotope label experiments with an isotope flux-balance model adapted from Leavitt et al. (2023). The model is informed by the enzymatic steps involved in the Wood-Ljungdahl (reductive acetyl-CoA) pathway used by *A. fulgidus* as well as archaeal isoprenoid lipid biosynthesis used by all tetraether-producing archaea. In addition to *A. fulgidus*, two thermoacidophilic archaea (*Acidianus* sp. DS80 and *Metallosphaera sedula* DSM 5348T) were grown in batch cultures for additional $\varepsilon_{L/W}$ measurements. We present

a synthesis of representative $\varepsilon_{L/W}$ values observed in Archaea, Bacteria, and Eukarya and discuss factors that may underlie some of the similarities observed across different domains of life.

2. Materials and Methods

2.1. Culture Strains and Growth

Archaeoglobus fulgidus str. VC-16 (DSM4304) was obtained from Deutsche Sammlung von Mikroorganismen und Zellkulturen (Braunschweig, Germany) and grown in batch cultures on two different carbon substrates and electron acceptors (Table 1). Culture media was prepared following the DSMZ 399 recipe with modifications as follows (per liter): 0.34 g KCl, 4.00 g $MgCl_2$ x 6 H_2O, 3.45 g $MgSO_4$ x 7 H_2O, 0.25 g NH_4Cl, 0.14 g $CaCl_2$ x 2 H_2O, 0.11 g K_2HPO_4 x 3 H_2O, 0.20 g KH_2PO_4, 18.00 g NaCl, 2.52 g $NaHCO_3$, 2 mL $Fe(NH_4)_2(SO_4)_2$ x 7 H_2O (0.1% w/v), and 10 mL trace element (DSMZ 141). After autoclaving, sterile anoxic solutions were added to the medium to a final concentration of 3.2 mM L-cysteine-HCl and 1% (v/v) vitamin (DSMZ 141). When thiosulfate was used as an electron acceptor, 4.00 g/L $MgCl_2$ x 6 H_2O and 3.45 g/L $MgSO_4$ x 7 H_2O were replaced with 4.70 g/L $MgCl_2$ x 6 H_2O and 3.48 g/L $Na_2S_2O_3$ x 5 H_2O. For heterotrophic growth, lactate was used as an electron donor and carbon source, 20 mM of Na-lactate solution was added and incubated with approximately 1 bar of N_2/CO_2 (80:20, v/v) headspace; for autotrophic growth, lactate was omitted and H_2 and CO_2 were used as an electron donor and carbon source, respectively, with 21 psig H_2/CO_2 (80:20, v/v) in the headspace. The headspace of autotrophic cultures were flushed and re-pressurized with H_2/CO_2 once per day after each OD measurement. The δ^2H of culture media was manipulated by volumetrically diluting 99.9 % purity ^2H_2O.

All cultures of *A. fulgidus* were incubated at 82 °C. Heterotrophic cultures were incubated statically, and autotrophic cultures were shaken at 200 rpm to increase gas exchange between the H_2/CO_2 headspace and culture media. The optical density at 600 nm (OD_{600}) of samples was used for monitoring growth, and linearity against direct cell counts was confirmed (depth 0.02 mm; Petroff-Hausser Counter 3900) throughout the absorbance range. Biomass samples were harvested twice per experiment, one during mid-exponential phase and the other during early stationary phase. To harvest, 50 mL of culture was centrifuged for 15 minutes at 4 °C and 4500 x *g*, and resulting wet cell pellets were stored at –80 °C until lipid extraction.

Batch cultures of *Acidianus* sp. DS80 and *M. sedula* DSM 5348T were grown for additional archaeal lipid $\varepsilon_{L/W}$ measurements (not for water isotope labeling experiments or isotope flux-balance model). *Acidianus* sp. DS80 was grown as previously described in Rhim et al. (2023), and *M. sedula* was grown in Brock basal salts medium with Allen's trace element mixture (Brock et al., 1972). See Supporting Information for additional details for growth conditions for *Acidianus* sp. DS80 and *M. sedula*.

2.2. Lipid Extraction, Ether Cleavage, and Quantification

Frozen cell pellets were lyophilized overnight, and dry cell pellets were extracted using acidic hydrolysis-methanolysis. Briefly, dry cell pellets were physically disrupted in 1.5-mL microcentrifuge tubes by vortexing with methanol (MeOH) and *ca*. 250 µL of 100 µm combusted glass beads for 10 minutes at 3000 rpm using a Disruptor Genie (Scientific 126 Industries, SI-DD38). After excess MeOH is evaporated, octacosanol (C_{28}) or lignocerol (C_{24}) and C_{46} GTGT were added to all samples as internal extraction standards. Samples were incubated at 65 °C for 90 minutes with 3 N methanolic HCl (33 % water content) to hydrolyze tetraether headgroups. Methyl tert butyl ether (MTBE) was added to the cooled samples at a ratio of 3:2 (acid:MTBE, v/v), and samples were sonicated for 5 minutes (Qsonica Q500, Newtown, CT, USA). After sonication, n-hexane was added at a 1:1 ratio (MTBE:hexane, v/v), vortexed, and centrifuged at 15,000 g for 3 minutes. The upper organic phase was collected three times with n-hexane for the two subsequent rounds. The resulting total lipid extracts (TLEs) were dried under N_2 and proceeded to ether cleavage or stored at –20 °C until ether cleavage.

Ether bonds were cleaved in 57% hydroiodic acid (HI) at 125 °C for 4 hours. Then the organic phase was collected three times using n-hexane. The resulting alkyl iodides were reduced to alkanes (biphytanes, BPs) with H_2 in the presence of $Pt^{(IV)}O_2$ (Kaneko et al., 2011). Hydrogenated samples were passed through combusted pasteur pipettes with glass wool plugs to remove PtO_2 powder. Filtered samples were dried under N_2 and stored at –20 °C until analysis. The resulting ether-cleaved BPs were analyzed on single quadrupole gas chromatography-mass spectrometer (GC-MS; Thermo ISQ LT with TRACE 1310) for compound identification and on GC-flame ionization detector (GC-FID; Thermo TRACE 1310) for quantification, both housed in the Organic Geochemistry Laboratory at the University of Colorado Boulder.

2.3. Hydrogen isotope analysis and data processing

The δ^2H of BPs was analyzed on a GC-pyrolysis-isotope ratio MS (GC-P-IRMS) on a GC IsoLink II IRMS System (Thermo Scientific) in the Organic Geochemistry Laboratory at the University of Colorado Boulder. The GC-P-IRMS system consists of a Trace 1310 GC fitted with a programmable temperature vaporization (PTV) injector and either a 30 m ZB5HT column (i.d. = 0.25 mm, 0.25 µm, Phenomenex, Torrance, CA, USA) or a 60 m DB1 column (i.d. = 0.25 mm, 0.25 µm, Agilent, Santa Clara, CA, USA), ConFlo IV interface, and MAT 253 Plus mass spectrometer (Thermo Scientific).

A. fulgidus has been observed to produce both tetraether and diether lipids, with the majority of GDGT with no ring (GDGT-0) and a small fraction with up to two pentacyclic rings (Lai et al., 2008). The tetraether-to-diether ratio for *A. fulgidus* is expected to be ~1:1 at the growth temperature in this study (82 °C; Lai et al., 2008), and we focus on the tetraether fraction for the

rest of the discussion. In line with the previous observation, the majority of BPs derived from *A. fulgidus* GDGT did not have rings (BP-0). All of the δ^2H values reported in this study are for BP-0.

All hydrogen isotope ratios are reported in the standard delta notation (δ^2H) in permil (‰) units, against the Vienna Standard Mean Ocean Water (VSMOW) international standard:

$$\delta\, 2H = \frac{(2H/1H)_{sample}}{(2H/1H)_{VSMOW}} - 1 \qquad \text{Eq. (1)}$$

The factor of 1000 is omitted from Eq. (1), following the IUPAC recommendations (Coplen, 2011). The lipid-water hydrogen isotope fractionation factor is reported in alpha notation ($^2\alpha_{L/W}$), and fractionation is reported in epsilon notation ($^2\varepsilon_{L/W}$) in ‰:

$$2\alpha_{L/W} = \frac{(2H/1H)_{lipid}}{(2H/1H)_{water}} \qquad \text{Eq. (2)}$$

$$2\varepsilon_{L/W} = 2\alpha_{L/W} - 1 \qquad \text{Eq. (3)}$$

Values of δ^2H were first determined relative to H_2 reference gas (δ^2H_{raw}), and then calibrated externally using a standard *n*-alkane mixture (A6, containing C_{15} through C_{30} n-alkanes spanning from –9 to –263 ‰ vs. VSMOW; A. Schimmelmann, Indiana University). The A6 standard was combined with a C_{36} n-alkane (nC_{36}, –259.2 ‰ vs. VSMOW; A. Schimmelmann, Indiana University) and measured at regular intervals at different concentrations. The BP δ^2H calibration was done in R, using the packages *isoreader* (Kopf et al., 2021) and *isoprocessor* available at github.com/isoverse. Details of the data reduction and calibration methods are described in Leavitt et al. (2022).

The δ^2H of the H_2 gas in H_2/CO_2 headspace of autotrophic cultures was analyzed on Thermo Gasbench II in the Stable Isotope Laboratory at Northwestern University. The δ^2H of non-exchangeable H in lactate used for heterotrophic cultures was assumed to be –60 ‰. The δ^2H of natural abundance and deuterium-enriched medium water was measured at the Stable Isotope Laboratory at Dartmouth College as previously described (Kopec et al., 2019). Briefly, water was reduced with chromium at 850 °C using the H-Device, and the δ^2H of the resulting gas was measured by an IRMS (Thermo Delta Plus XL). The measured δ^2H values were converted to the water δ^2H equivalent by calibrating with water standards with known isotopic compositions analyzed in the same way. For samples expected to be outside the range of the standards (e.g., the deuterium-enriched medium), samples were diluted with water standards. The 1σ uncertainty for δ^2H measurements is 0.5 ‰.

2.4. Model implementation

An isotope flux-balance model was adapted from the conceptual framework described in Leavitt et al. (2023). Our model considers the Wood-Ljungdahl (reductive acetyl-CoA) pathway used by *A. fulgidus* for determining the sources and fluxes of H during acetyl-CoA (Ac-CoA) synthesis. It also considers the general archaeal lipid biosynthesis pathway for the accounting of total H budget in archaeal lipids. Analytical solutions for Eqn. 5–12 were obtained via R. Details of the model design and outcomes are described in section 4.

3. Results

3.1. Cultures and growth rates

Archaeoglobus fulgidus is a metabolically flexible strain from the phylum Euryarchaeota. We cultivated *A. fulgidus* in batch (closed-system) cultures on three different combinations of electron donors and acceptors (Table 1; Fig. 1A–C). In two treatments, *A. fulgidus* was grown as a heterotroph, using lactate as the carbon source and electron donor and sulfate or thiosulfate as the terminal electron acceptor. In the third treatment, *A. fulgidus* was grown as an autotroph, using CO_2 as the carbon source, H_2 as the electron donor, and thiosulfate as the terminal electron acceptor. Cultures were acclimated to each treatment by growing on respective substrate combinations for two or more passages before inoculation. Overall, heterotrophic conditions resulted in faster growth (T-L, t_d = 6.2 ± 0.6 h; S-L, t_d = 10.3 ± 1.7 h) compared to autotrophic growth (T-H_2/CO_2, t_d = 19.3 ± 3.9 h) (Table 1; Fig. 1A–B).

Table 1. Summary of culture experiments.

Experimental Condition	electron donor	electron acceptor	carbon source	t_d (h)
Thiosulfate-Lactate (T-L)	Lactate (20 mM)	Thiosulfate (14 mM)	Lactate (20 mM)	6.2 ± 0.6
Sulfate-Lactate (S-L)	Lactate (20 mM)	Sulfate (14 mM)	Lactate (20 mM)	10.3 ± 1.7
Thiosulfate-H_2/CO_2 (T-H_2/CO_2)	H_2 (g)* (80% v/v)	Thiosulfate (14 mM)	CO_2 (g)* (20% v/v)	19.3 ± 3.9

* The headspace of autotrophic cultures was filled with 21 psig H_2/CO_2 (80:20, v/v) and re-pressurized with H_2/CO_2 once per day after each OD measurement.

3.2. Carbon metabolism and growth phase affect lipid δ^2H and regression parameters

Different modes of carbon metabolism in *A. fulgidus* not only resulted in different growth rates (Table 1) but also affected lipid δ^2H and regression parameters. The lipid isotopic composition reflects the sum of distinct isotope fractionations between lipid and each external H source, resulting in the isotopic mass balance (Zhang et al., 2009):

$$R_{BP} = f_W \cdot 2\alpha_{L/W} \cdot R_W + f_S \cdot 2\alpha_{L/S} \cdot R_S \qquad \text{Eq. (4)}$$

where R_{BP}, R_W, and R_S represent the $^2H/^1H$ ratios of BPs from GDGT-0 (BP-0), media water, and substrate (lactate for the heterotrophic conditions; H_2 for the autotrophic condition), respectively. f_W and f_S are the fractions of lipid-bound H originating from water and substrate, respectively. $^2\alpha$ represents the net isotope fractionation factor between lipid and water ($^2\alpha_{L/W}$) and between lipid and substrate ($^2\alpha_{L/S}$), respectively. In parallel cultures where only one parameter (R_W) is varied experimentally, measurements of R_L, R_W, and R_S provide the basis for regression of R_L on R_W. The isotope analysis results and regression parameters are summarized in Table 2.

The δ^2H_L values were strongly correlated with δ^2H_W values in all experiments (Table 2; $R^2 \geq 0.993$ and $p \leq 0.05$ in every regression). The regression slopes varied as a function of carbon metabolism and growth phase. Overall, the two heterotrophic conditions (T-L and S-L) and exponential growth phase resulted in lower slopes compared to the autotrophic condition (T-H_2/CO_2) and stationary growth phase. Slopes for the two heterotrophic conditions were comparable (0.481 for T-L, 0.477 for S-L during exponential phase; 0.548 for T-L, 0.519 for S-L during stationary phase; Table 2). The autotrophic condition resulted in higher slopes (0.552, exponential phase; 0.628, stationary phase). Notably, the higher slope observed during the stationary phase of the autotrophic culture was the closest to the slope estimated assuming $f_W = 1$ (0.707) (Table 2; Fig. 1D).

Table 2. Data for tetraether-derived biphytanes produced by *Archaeoglobus fulgidus* grown on different carbon substrates and electron donor-acceptor pairs.

Substrate [a]	Growth Phase [b]	Avg. OD[c]	δ^2H_W[d] (‰)	s.d. (‰)	δ^2H_L[e] (‰)	s.d. (‰)	$^2\varepsilon_{L/W}$ (‰)	s.d. (‰)	n[f]	Slope[g] ($^2\alpha_{L/W} \cdot f_W$)	R^2	*p*
T-L	Exp	0.147	362.4	0.2	–70.7	6.6	–317.9	29.4	3	0.481	0.996	1×10^{-7}
		0.135	176.0	0.2	–164.6	7.0	–289.6	12.4	3			
		0.141	–64.0	0.2	–275.8	7.1	–226.2	5.9	2			
	Exp+Sta	0.346	361.3	0.2	–52.7	6.7	–304.1	38.5	2	0.548	0.999	3×10^{-6}
		0.344	175.5	0.2	–152.4	7.5	–279.0	13.7	2			
		0.351	–63.7	0.2	–285.3	8.7	–236.7	7.2	2			
S-L	Exp	0.096	361.8	0.2	–87.5	9.7	–329.9	36.4	1	0.477	0.993	7×10^{-5}
		0.100	174.7	0.2	–163.5	4.8	–287.9	8.5	3			
		0.082	–61.7	0.2	–289.7	5.9	–243.0	5.0	2			
	Exp+Sta	0.307	361.4	0.2	–66.9	5.7	–314.6	26.9	2	0.519	0.998	4×10^{-7}
		0.295	175.4	0.2	–168.1	4.9	–292.3	8.5	2			
		0.282	–61.5	0.2	–287.1	10.2	–240.3	8.6	2			
T-H_2/CO_2	Exp	0.052	348.3	0.2	–72.8	5.0	–312.3	21.5	2	0.552	0.998	8×10^{-5}
		0.046	164.8	0.2	–176.8	7.0	–294.0	11.5	1			
		0.054	–66.5	0.2	–302.1	4.7	–252.4	4.0	1			
	Exp+Sta	0.137	348.5	0.2	–71.7	8.7	–311.7	37.8	3	0.628	0.997	1×10^{-5}
		0.132	166.0	0.2	–173.8	10.0	–291.4	16.8	1			
		0.134	–64.5	0.2	–326.4	10.2	–279.9	8.8	2			
T-H_2/CO_2 (calculated)	-	-	-	-	-	-	-	-	-	*0.707 (f_W = 1)*	-	-

[a] Thiosulfate-lactate (T-L); sulfate-lactate (S-L); thiosulfate-H_2/CO_2 (T-H_2/CO_2)
[b] Biomass harvested during mid-exponential growth phase (Exp); biomass harvested during early stationary phase, including biomass from both exponential and stationary phase (Exp+Sta)
[c] Optical density (OD)
[d] δ^2H of culture medium at the time of biomass sampling. Average of biological and technical replicates ± 1 s.d.
[e] Weighted mean δ^2H of biphytane from GDGT-0
[f] Number of biological replicates used to calculate the average values of δ^2H_{Water}, δ^2H_{Lipid}, and $^2\varepsilon_{L/W}$
[g] Slope for the regression of δ^2H_{Lipid} against δ^2H_{Water} (*see* Figure 1D-F)

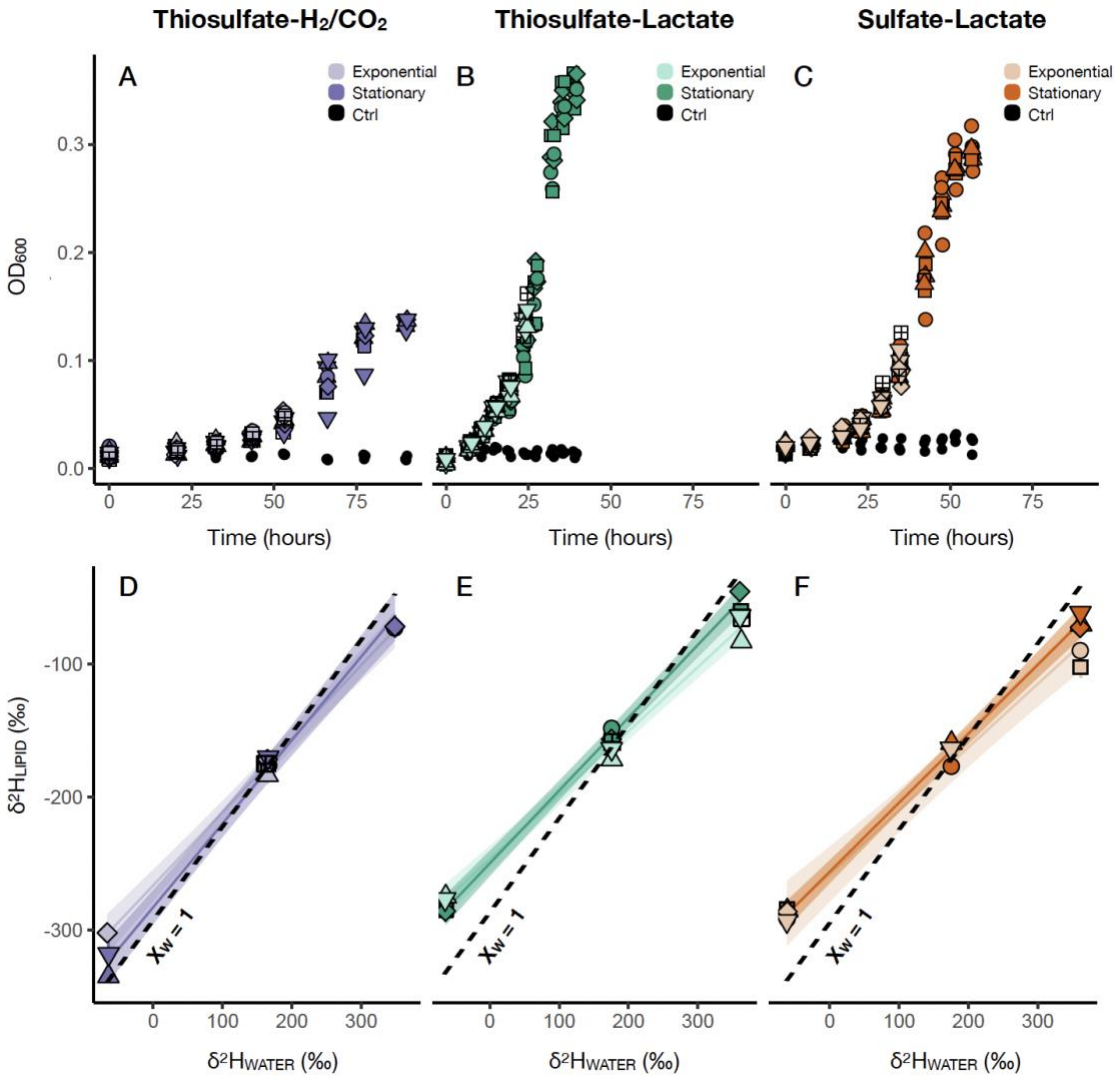

Figure 1. Growth curves and regression of lipid δ^2H versus water δ^2H for *Archaeoglobus fulgidus*. Growth curves of *A. fulgidus* grown autotrophically on (A) thiosulfate and H_2/CO_2 or heterotrophically on (B) thiosulfate and lactate or (C) sulfate and lactate. Regression of biphytane hydrogen isotopic composition (δ^2H_L) on water isotopic composition (δ^2H_W) grown on (D) thiosulfate and H_2/CO_2, (E) thiosulfate and lactate, and (F) sulfate and lactate.

4. *A. fulgidus* H-isotope flux-balance model

To further interpret these findings, we modified the isotope flux-balance model recently developed for an ammonia-oxidizing archaeon *N. maritimus* SCM1 (Leavitt et al., 2023) to reflect the biochemistry underlying the carbon metabolism modes in *Archaeoglobus fulgidus* VC-16. The overall conceptual framework consists of two parts for the stoichiometric accounting of: 1) methyl-H in Ac-CoA and 2) the 80 H atoms in the C_{40} alkyl chain of BPs inherited from Ac-CoA. The former requires metabolism-specific information considering the mode(s) of carbon fixation and

experimental conditions such as substrate availability, while the latter is informed by more universal information about archaeal isoprenoid biosynthesis. Below, we describe the details of the two parts of our model.

4.1. Sources of lipid-H via the modified Wood-Ljungdahl pathway

4.1.1. Heterotrophy

A. fulgidus can grow autotrophically or heterotrophically via the modified reductive Ac-CoA or Wood-Ljungdahl pathway (Möller-Zinkhan et al., 1989; Möller-Zinkhan and Thauer, 1990; Hocking et al., 2014). During chemoorganoheterotrophic growth on lactate, the type species *A. fulgidus* VC16 couples the complete oxidation of organic substrates to CO_2 with the reduction of sulfate or thiosulfate to sulfide. In this study, the organic substrate was lactate. *A. fulgidus* oxidizes lactate via pyruvate and Ac-CoA using enzymes and cofactors involved in the C_1-pathway, similar to those found in methanogens, in reverse direction (Fig. 2A; Möller-Zinkhan et al., 1989; Möller-Zinkhan and Thauer, 1990). A D-lactate dehydrogenase in *A. fulgidus* catalyzes the first step of lactate oxidation to pyruvate coupled with the reduction of menaquinone (MQ), resulting in menaquinol (MQH_2) (Step 1, Fig. 2A; Kunow et al., 1993; Reed and Hartzell, 1999). The next step of pyruvate oxidation to Ac-CoA is catalyzed by pyruvate:ferredoxin oxidoreductase (Step 2, Fig. 2A; Kunow et al., 1993). The 3 H atoms in the methyl group of lactate most likely remain intact and are inherited to Ac-CoA. Some of these Ac-CoA products are used for biomass synthesis (Step 3.2, Fig. 2A), including isoprenoid lipid biosynthesis, while some of them are degraded further for the complete oxidation of lactate. For the latter, carbon monoxide dehydrogenase catalyzes both the reversible carbon-carbon cleavage of Ac-CoA and the oxidation of carbonyl group to CO_2 coupled with ferredoxin (Fd) reduction (Step 3.1, Fig. 2A; Möller-Zinkhan and Thauer, 1990).

The coenzymes involved in the downstream oxidative branch of Ac-CoA degradation could transfer hydrides (e.g., $F_{420}H_2$ in Steps 4 and 5, Fig. 2A). These fluxes of H are important to track, because the hydrides from Ac-CoA (ultimately from lactate) can be recycled for NADP reduction, the product of which (NADPH) can donate hydrides to isoprenoid precursors during lipid biosynthesis (i.e., contribution of lactate-derived H to lipids). We assign F_{420} and Fd as the electron acceptors for Steps 4–5 and Step 8, respectively (Fig. 2A), given that the genes relating to all steps of the reductive Ac-CoA pathway are expressed in *A. fulgidus* (Hocking et al., 2014) and considering the known mechanisms of how the enzymes of interest operate in methanogens. In CO_2-reducing methanogens, both methylenetetrahydromethanopterin reductase (Mer) and methylenetetrahydromethanopterin dehyrogenase (Mtd) oxidize $F_{420}H_2$ (Steps 4 and 5, respectively, in reverse; Fig. 2A), and formylmethanofuran dehydrogenase (Fwd) requires Fd_{red} (Step 8, in reverse; Fig. 2A) (Thauer et al., 2010).

4.1.2. Autotrophy

During chemolithoautotrophic growth, the type species *A. fulgidus* VC16 couples the oxidation of H_2 or formate with the reduction of thiosulfate or sulfite (Stetter, 1988; Steinsbu et al., 2010). In this study, H_2 and thiosulfate were used as electron donor and acceptor for the autotrophic condition (T-H_2/CO_2). *A. fulgidus* reduces CO_2 to synthesize Ac-CoA via the C_1-pathway (Fig. 2B), in principle a reversal of the Ac-CoA degradation during heterotrophy (Fig. 2A). The same enzymes involved in H additions used by CO_2-reducing methanogens catalyze the successive addition of H during autotrophic carbon fixation in *A. fulgidus*: Fwd (Step 1), Mtd (Step 4), and Mer (Step 5) (Fig. 2B). During chemolithoautotrophy, the H atoms in methyl precursors in theory derive from intracellular water. However, one of the isoenzymes for methylenetetrahydromethanopterin (CH_2-H_4MPT) dehydrogenase is H_2-dependent (Hmd) and uses H_2 directly, as opposed to $F_{420}H_2$ used by the other isoenzyme Mtd, to reduce methyl-H_4MPT (Hendrickson and Leigh, 2008). Given the similarities between methanogens and *A. fulgidus*, we consider the possible flux of H from H_2 to Ac-CoA (Step 4–6, Fig. 2B) in one of the end-member scenarios (see 4.2; Table 3).

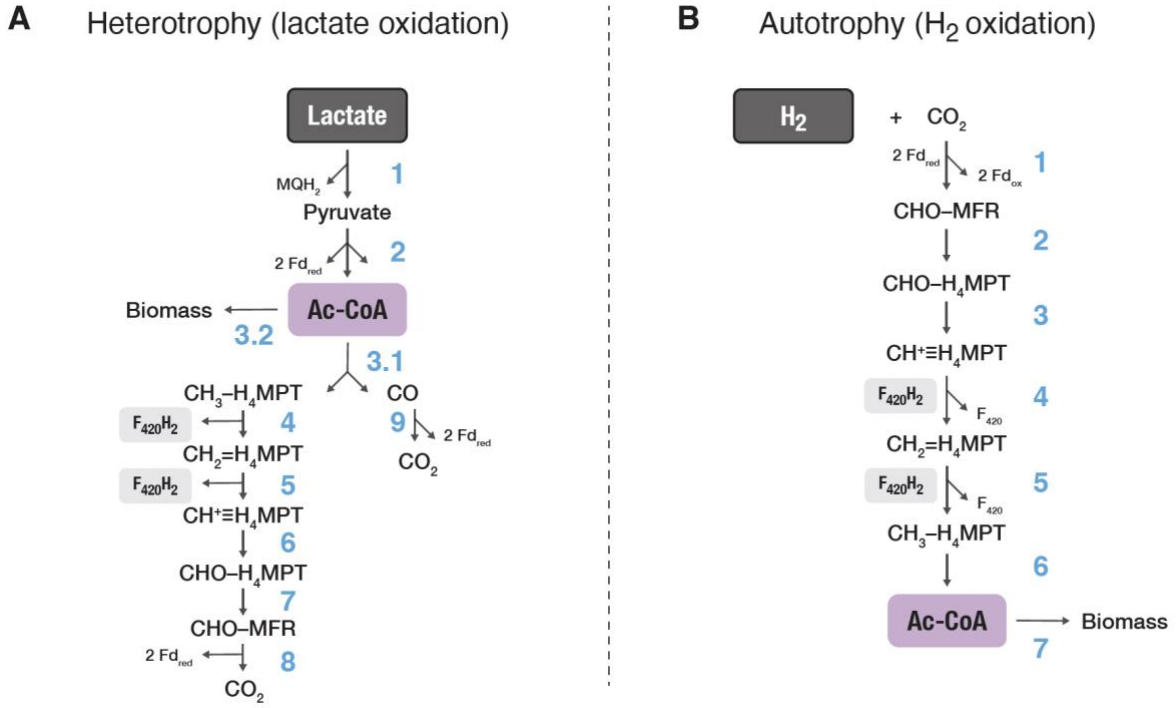

Figure 2. Carbon metabolism by *Archaeoglobus fulgidus* via the modified reductive acetyl-CoA or Wood-Ljungdahl pathway. (A) Chemoorganoheterotrophic growth on lactate: lactate is oxidized via pyruvate and acetyl-CoA, which either serves as the building blocks for biosynthesis or is further degraded for the complete oxidation of lactate. (B) Chemolithoautotrophic growth on H_2/CO_2: CO_2 is reduced to produce acetyl-CoA via the C_1-pathway, with enzymes and cofactors similar to those involved in methanogenesis. Abbreviations: MQH_2, menaquinol or reduced menaquinone; Fd_{red}, reduced ferredoxin; Ac-CoA, acetyl-CoA; CH_3-H_4MPT, methyl-tetrahydromethanopterin (H_4MPT); CH_2=H_4MPT, methylene-H_4MPT; CH^+≡H_4MPT, methenyl-H_4MPT; CHO-H_4MPT, formyl-H_4MPT; CHO-MFR, formylmethanofuran; $F_{420}H_2$, reduced coenzyme F_{420}.

4.2. Model schematics and stoichiometric accounting

Fractions of Ac-CoA produced via the modified Wood-Ljungdahl pathway described above are used for the synthesis of archaeal isoprenoids. Leavitt et al. (2023) provides a detailed overview of the sources of H and mechanisms of the biochemical steps involved in archaeal tetraether biosynthesis (Supporting Information, Fig. S1). In short, the mevalonate pathway synthesizes isopentenyl pyrophosphate (IPP), which are C_5 isoprene units, from three units of Ac-CoA. Then, three units of IPP and its isomer condense to yield the C_{20} precursor, geranylgeranyl diphosphate (GGPP). The geranylgeranyl chains are transferred around to yield di-O-geranylgenranylglyceryl phosphate (DGGGP) with the glycerol-1-phosphate (G1P) backbone. The tetraether synthase (Tes) enzyme catalyzes the condensation of two DGGGP units to yield the membrane-spanning tetraether. Finally, the geranylgeranyl reductase (GGR) enzyme catalyzes the saturation of tetraether to yield GDGT. We combine the stoichiometric accounting of the methyl-H in Ac-CoA for *A. fulgidus* (see 4.1) and of the 80 H atoms in the C_{40} alkyl chain of BPs inherited from Ac-CoA during tetraether biosynthesis described above (Leavitt et al., 2023) to build an overall schematics of the specific model scenarios explored in this study (Fig. 3).

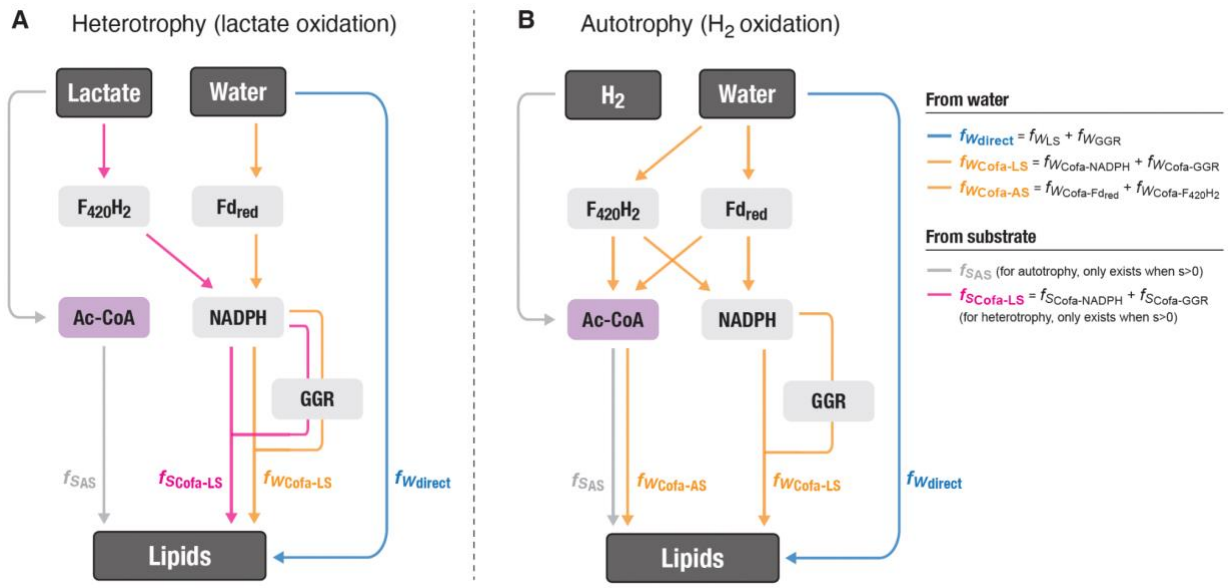

Figure 3. Schematic diagram of the isotope flux-balance model for *Archaeoglobus fulgidus*. (A) Heterotrophic scenario for lactate oxidation; (B) autotrophic scenario for H_2 oxidation. Color codes for the different H fluxes (*f*) are shown in the legend. The subscript W stands for water as the ultimate H source; the subscript S stands for substrate as the ultimate H source, where the substrates are lactate and H_2 for heterotrophy and autotrophy, respectively. See 4.2.1 and Eq. 5–8 for detailed descriptions of individual fluxes. Abbreviations: LS, lipid synthesis; AS, acetyl-CoA synthesis; Cofa, cofactor; $F_{420}H_2$, reduced coenzyme F_{420}; Fd_{red}, reduced ferredoxin; Ac-CoA, acetyl-CoA; GGR, geranylgeranyl reductase.

4.2.1. Overview of hydrogen budget

In our model for *A. fulgidus*, we consider two ultimate sources of H for both heterotrophic and autotrophic model cases: water and substrate. Water refers to intracellular water for both cases, and water-derived H can be conceptualized as either direct incorporation of intracellular water or donation from reducing cofactors. Substrate refers to lactate and H_2, respectively, for the heterotrophic (Fig. 3A) and autotrophic cases (Fig. 3B). The stoichiometric budget for H sources in *A. fulgidus* can be simplified with the following fractions that make up either of the two passages for water H incorporation and substrate H incorporation. For the 80 H atoms in BP produced via heterotrophy (BP_{Het}): H derived directly from water via lipid biosynthesis ($f_{W,LS}$) and GGR reduction ($f_{W,GGR}$) are combined to yield total direct water H ($f_{W,direct}$); H derived indirectly from water via reducing cofactors NADPH ($f_{W,Cofa\text{-}NADPH}$) and GGR ($f_{W,Cofa\text{-}GGR}$) are combined to yield total indirect water H during lipid synthesis ($f_{W,Cofa\text{-}LS}$); H derived indirectly from lactate (substrate) via reducing cofactors NADPH ($f_{S,Cofa\text{-}NADPH}$) and GGR ($f_{S,Cofa\text{-}GGR}$) are combined to yield total indirect water H during lipid synthesis ($f_{S,Cofa\text{-}LS}$); and H derived directly from lactate during Ac-CoA synthesis ($f_{S,AS}$).

$$BP_{Het} = f_{W,direct} + f_{W,Cofa\text{-}LS} + f_{S,Cofa\text{-}LS} + f_{S,AS} \quad \text{Eq. (5a)}$$

$$BP_{Het} = (f_{W,LS} + f_{W,GGR}) + (f_{W,Cofa\text{-}NADPH} + f_{W,Cofa\text{-}GGR}) + (f_{S,Cofa\text{-}NADPH} + f_{S,Cofa\text{-}GGR}) + f_{S,AS} \quad \text{Eq. (5b)}$$

For the 80 H atoms in BP produced via autotrophy (BP_{Auto}): H derived directly from water via lipid biosynthesis ($f_{W,LS}$) and GGR reduction ($f_{W,GGR}$) are combined to yield total direct water H ($f_{W,direct}$); H derived indirectly from water via reducing cofactors NADPH ($f_{W,Cofa\text{-}NADPH}$) and GGR ($f_{W,Cofa\text{-}GGR}$) are combined to yield total indirect water H during lipid synthesis ($f_{W,Cofa\text{-}LS}$); H derived indirectly from water via reducing cofactors Fd_{red} ($f_{W,Cofa\text{-}Fdred}$) and $F_{420}H_2$ ($f_{W,Cofa\text{-}F420H2}$) are combined to yield total indirect water H during Ac-CoA synthesis ($f_{W,Cofa\text{-}AS}$); and H derived directly from H_2 (substrate) via Ac-CoA synthesis ($f_{S,AS}$).

$$BP_{Auto} = f_{W,direct} + f_{W,Cofa\text{-}LS} + f_{W,Cofa\text{-}AS} + f_{S,AS} \quad \text{Eq. (6a)}$$

$$BP_{Auto} = (f_{W,LS} + f_{W,GGR}) + (f_{W,Cofa\text{-}NADPH} + f_{W,Cofa\text{-}GGR}) + (f_{W,Cofa\text{-}Fdred} + f_{W,Cofa\text{-}F420H2}) + f_{S,AS} \quad \text{Eq. (6b)}$$

These fractions represent the relative fluxes of H (i.e., individual arrows either directly or indirectly connecting the two ultimate H sources, water and substrate, to lipids) shown in Fig. 3. We explore four scenarios for each case to explore the degree of water exchange, x_{ex}, ranging from 0% of minimal exchange to 100% of maximal exchange and the degree of substrate contribution, ranging from 0% of minimal contribution to 100% of maximal contribution. For the heterotrophic case, the assigned fractions are as follows (Eq. 7):

$$f_{W,LS} = \left[\frac{2}{3} \cdot (1 - x_{ex}) + 24 \cdot x_{ex}\right] \div 80$$

$$f_{W,GGR} = 8 \div 80$$

$$f_{W,direct} = \left[\frac{2}{3} \cdot (1 - x_{ex}) + 24 \cdot x_{ex} + 8\right] \div 80$$

$$f_{W,cofa-NADPH} = \left[16 \cdot (1 - \frac{1}{3} \cdot s)\right] \div 80$$

$$f_{W,cofa-GGR} = \left[8 \cdot (1 - \frac{1}{3} \cdot s)\right] \div 80$$

$$f_{W,cofa-LS} = \left[(16 + 8) \cdot (1 - \frac{1}{3} \cdot s)\right] \div 80$$

$$f_{S,cofa-NADPH} = \left[16 \cdot \frac{1}{3} \cdot s\right] \div 80$$

$$f_{S,cofa-GGR} = \left[8 \cdot \frac{1}{3} \cdot s\right] \div 80$$

$$f_{S,cofa-LS} = \left[(16 + 8) \cdot (\frac{1}{3} \cdot s)\right] \div 80$$

$$f_{S,AS} = \left[24 + \left(23 + \tfrac{1}{3}\right) \cdot (1 - x_{ex})\right] \div 80 \quad \text{Eq. (7)}$$

where x_{ex} is the degree of water exchange during lipid synthesis, which depends on the extent of re-equilibration during isomerization steps (steps 2 and 6; Supporting Information, Fig. S1). The s term is the degree of H contribution to lipids from substrate (lactate). Fractions that contain the x_{ex} term ($f_{W,direct}$ and $f_{S,AS}$; Eq. 7) vary between the two end-member scenarios of x_{ex} = 0 % (minimal exchange) and x_{ex} = 100 % (maximal exchange); fractions that contain the s term ($f_{W,cofa\text{-}LS}$ and $f_{S,cofa\text{-}LS}$; Eq. 7) vary between the two end-member scenarios of s = 0 % (minimal contribution) and s = 100 % (maximal contribution). At maximal substrate contribution (s = 100 %), ⅓ of $f_{W,cofa\text{-}LS}$

and $f_{S,cofa\text{-}LS}$ fractions derive from substrate H. During the complete oxidation of lactate to CO_2, the average carbon oxidation state increases from 0 to +4 (i.e., 12 electrons transferred total for all three carbons per molecule of lactate). The electron acceptors for the six oxidation steps are: menaquinone, for lactate to pyruvate oxidation (step 1; Fig. 2A); ferredoxin, for pyruvate to Ac-CoA oxidation and the final two oxidation steps to CO_2 (steps 3, 8 and 9; Fig. 2A); and F_{420}, for methenyl-H_4MPT and methylene-H_4MPT oxidation (steps 4 and 5; Fig. 2A) (Möller-Zinkhan et al., 1989; Schmitz et al., 1991; Klein et al., 1993; Kunow et al., 1993; Schwörer et al., 1993). None of these redox reactions during lactate oxidation involve NAD or NADP as electron acceptors; in *A. fulgidus*, reduced pyridine nucleotides (NADPH) required for biosynthesis is produced via the reversible reduction of NADP with $F_{420}H_2$, similar to the case in methanogens (Kunow et al., 1993). Therefore, in the maximal substrate contribution scenario (s = 100 %), up to ⅓ of H fluxes through the cofactor NADPH and GGR can derive from the two (out of six, hence ⅓) lactate-derived $F_{420}H_2$ that donate hydrides to NADP ($f_{S,cofa\text{-}LS}$; Fig. 3A).

For the autotrophic case, the assigned fractions are as follows (Eq. 8):

$$f_{W,LS} = \left[\frac{2}{3}\cdot(1-x_{ex}) + 24\cdot x_{ex}\right] \div 80$$
$$f_{W,GGR} = 8 \div 80$$
$$f_{W,direct} = \left[\frac{2}{3}\cdot(1-x_{ex}) + 24\cdot x_{ex} + 8\right] \div 80$$
$$f_{W,Cofa-NADPH} = 16 \div 80$$
$$f_{W,Cofa-GGR} = 8 \div 80$$
$$f_{W,Cofa-LS} = (16+8) \div 80$$
$$f_{W,Cofa-Fdred} = \frac{1}{3}\cdot\left[24 + \left(23+\frac{1}{3}\right)\cdot(1-x_{ex})\right] \div 80$$
$$f_{W,Cofa-F420H2} = \left[\frac{1}{3}\cdot\left[24 + \left(23+\frac{1}{3}\right)\cdot(1-x_{ex})\right]\right]\cdot(2-s) \div 80$$
$$f_{W,Cofa-AS} = \left[\frac{1}{3}\cdot\left[24 + \left(23+\frac{1}{3}\right)\cdot(1-x_{ex})\right] + \left[\frac{1}{3}\cdot\left[24 + \left(23+\frac{1}{3}\right)\cdot(1-x_{ex})\right]\right]\cdot(2-s)\right] \div 80$$
$$f_{S,AS} = \frac{1}{3}\cdot s\cdot\left[24 + \left(23+\frac{1}{3}\right)\cdot(1-x_{ex})\right] \div 80 \qquad \text{Eq. (8)}$$

where x_{ex} is the same as above (degree of water exchange during lipid synthesis, and s is the degree of H contribution to lipids from substrate, H_2. Similar to the heterotrophic case above, the same four scenarios with end-member values of x_{ex} and s are applied to the autotrophic case. Here, the three reduction steps involved in autotrophic Ac-CoA synthesis (steps 1, 4 and 5; Fig. 2B) are the reverse of oxidative Ac-CoA degradation during heterotrophy (steps 4, 5 and 8; Fig. 2A). The first reduction step (step 1, Fig. 2B) involves Fd_{red}, and the next two reduction steps (steps 4 and 5, Fig. 2B) involve $F_{420}H_2$, where H in both of these electron donors derive from water ($f_{W,cofa\text{-}AS}$, Fig. 3B). For the autotrophic case, we assign the maximal substrate contribution (s = 100 %) when the H_2-dependent isoenzyme, Hmd, catalyzes the methenyl-H_4MPT reduction (step 4, Fig. 2B) under

high partial pressure of H_2 (see 4.1.2). In this case, one of the three methyl-H in Ac-CoA derives directly from H_2 ($f_{S,AS}$, Fig. 3B).

4.2.2. Empirically informed isotopic mass balance

With the fractions defined in the hydrogen budget (see 4.2.1), the isotopic mass balance in Eq. (4) can be further refined. Replacing the f_W and f_S terms in Eq. (4) with the sums of all water-derived and lactate-derived fractions in Eq. (5), isotopic mass balance for the heterotrophic case becomes:

$$R_{BP,het} = \left(f_{W,direct} \cdot \alpha_{W,direct} + f_{W,cofa-LS} \cdot \alpha_{W,cofa-LS}\right) \cdot R_W + \left(f_{S,cofa-LS} \cdot \alpha_{S,cofa-LS} + f_{S,AS} \cdot \alpha_{S,AS}\right) \cdot R_S \quad \text{Eq. (9)}$$

Similarly, isotopic mass balance for the autotrophic case becomes:

$$R_{BP,auto} = \left(f_{W,direct} \cdot \alpha_{W,direct} + f_{W,cofa-AS} \cdot \alpha_{W,cofa-AS} + f_{W,cofa-LS} \cdot \alpha_{W,cofa-LS}\right) \cdot R_W + f_{S,AS} \cdot \alpha_{S,AS} \cdot R_S \quad \text{Eq. (10)}$$

Now we can use the regression parameters estimated from the δ^2H_{H2O} label experiments (Fig. 1; Table 2) to calculate analytical solutions for reasonable ranges of individual terms in Eq. (9–10). In Eq. (9–10), the coefficient for R_W in the first term represents the slope, *m*, and the entire second term represents the intercept, *c*. For heterotrophy:

$$m_{het} = f_{W,net} \cdot \alpha_{W,net} = f_{W,direct} \cdot \alpha_{W,direct} + f_{W,cofa-LS} \cdot \alpha_{W,cofa-LS}$$
$$\varepsilon_{W,net} = \frac{m_{het}}{f_{W,net}} - 1 = \frac{f_{W,direct} \cdot \alpha_{W,direct} + f_{W,cofa-LS} \cdot \alpha_{W,cofa-LS}}{f_{W,net}} - 1 \quad \text{Eq. (11)}$$

$$c_{het} = f_{S,net} \cdot \alpha_{S,net} \cdot R_S = f_{S,cofa-LS} \cdot \alpha_{S,cofa-LS} + f_{S,AS} \cdot \alpha_{S,AS}$$
$$\varepsilon_{S,net} = \frac{c_{het}}{f_{S,net} \cdot R_S} - 1 = \frac{f_{S,cofa-LS} \cdot \alpha_{S,cofa-LS} + f_{S,AS} \cdot \alpha_{S,AS}}{f_{S,net}} - 1 \quad \text{Eq. (12)}$$

where $\varepsilon_{W,net}$ and $\varepsilon_{S,net}$ refer to the net isotope fractionation between water and lipid (combining isotope effects associated with the water-derived fluxes, $f_{W,direct}$ and $f_{W,cofa-LS}$) and between substrate and lipid (combining isotope effects associated with the substrate-derived fluxes, $f_{S,cofa-LS}$ and $f_{S,AS}$), respectively.

4.3. Model results

Table 3, Fig. 4 and 5 shows the summary of model results. We first estimated $f_{W,net}$, which we define as the net total contribution of H from water to lipids ($f_{W,net} = f_{W,direct} + f_{W,cofa}$), for a range of x_{ex} from 0 % to 100 %. Overall, the autotrophic case had a higher range of $f_{W,net}$ compared to the two heterotrophic cases (Table 3; Fig. 4A–C). Even for the minimal water exchange and maximal substrate contribution scenario (x_{ex} = 0 %, *s* = 100 %), when the contribution from water

is expected to be the lowest, $f_{W,net}$ was 80 % (Table 3; dashed line, Fig. 4C). For the two heterotrophic cases, the $f_{W,net}$ values were 31 and 70 % for the lowest (x_{ex} = 0 %, s = 100 %) and highest (x_{ex} = 100 %, s = 0 %) water contribution scenarios, respectively (Table 3; Fig. 4A–B).

For the net isotope fractionation between lipid and water ($\varepsilon_{W,net}$), the two heterotrophic cases showed similar ranges and patterns where the $\varepsilon_{W,net}$ values decrease with increasing x_{ex} (Fig. 4D–E). The $\varepsilon_{W,net}$ range was relatively more positive during stationary growth phase (–218 to 776 ‰ for the T-L condition; –259 to 682 ‰ for the S-L condition) compared to exponential growth phase (–312 to 561 ‰ for the T-L condition; –319 to 546 ‰ for the S-L condition) (Table 3; Fig. 4D–E). For the autotrophic case, the growth phase-dependent trend was also observed (more positive $\varepsilon_{W,net}$ during stationary phase; Table 3; Fig. 4F). Unlike in the heterotrophic cases, all $\varepsilon_{W,net}$ values for the autotrophic case were negative and fell within a relatively narrow range for the entire range of x_{ex} (–448 to –312 ‰ for exponential phase; –372 to –228 ‰ for stationary phase; Table 3). For the autotrophic case, a theoretical end-member $\varepsilon_{W,net}$ with no substrate contribution can be estimated by calculating the regression slope through the origin (i.e., no intercept, which represents the substrate contribution term, $f_S \cdot {}^2\alpha_{L/W} \cdot R_S$; Eq. 4): –293 ‰ for the autotrophic case (magenta line; Fig. 4F). This value falls within the range of $\varepsilon_{W,net}$ for stationary, rather than exponential, growth phase (Fig. 4F). For the net isotope fractionation between lipid and substrate ($\varepsilon_{S,net}$), the two heterotrophic cases showed similar ranges and patterns where $\varepsilon_{S,net}$ values increase with increasing x_{ex} (Fig. 4G–I). The growth phase-dependent trend for $\varepsilon_{S,net}$ contrasted that of $\varepsilon_{W,net}$, where the $\varepsilon_{S,net}$ range was relatively more negative during stationary growth phase (–688 to –282 ‰ for the T-L condition; –654 to –201 ‰ for the S-L condition) compared to exponential growth phase (–582 to –36 ‰ for the T-L condition; –592 to –59 ‰ for the S-L condition) (Table 3; Fig. 4G–H). A similar trend was observed for the autotrophic case (more negative $\varepsilon_{S,net}$ during stationary phase; Table 3; Fig. 4I).

The net isotope fractionation factors ($\varepsilon_{W,net}$ and $\varepsilon_{S,net}$) can be further broken down into individual fluxes associated with water-derived and substrate-derived H atoms, respectively. The net isotope fractionation factor between lipid and water ($\varepsilon_{W,net}$) can be divided into: 1) $\varepsilon_{W,direct}$ associated with water-derived H atoms that are transferred through the $f_{W,direct}$ flux (Fig. 3) via H exchange between isoprenoid precursors and intracellular water or addition via GGR, and 2) $\varepsilon_{W,cofa}$ associated with the $f_{W,cofa}$ flux ($f_{W,cofa\text{-}LS}$ for heterotrophy; $f_{W,cofa\text{-}LS}$ and $f_{W,cofa\text{-}AS}$ for autotrophy; Fig. 3) via cofactors (Fd_{red} and $F_{420}H_2$ for autotrophy; Fd_{red} for heterotrophy) (Fig. 5A–C). The net isotope fractionation factor between lipid and substrate ($\varepsilon_{S,net}$) can be divided into: 1) $\varepsilon_{S,AS}$ associated with substrate-derived H atoms that are transferred through the $f_{S,AS}$ flux (Fig. 3) via Ac-CoA synthesis, and 2) $\varepsilon_{S,cofa}$ associated with the $f_{S,cofa}$ flux ($f_{S,cofa\text{-}NADPH}$ and $f_{S,cofa\text{-}GGR}$ for heterotrophy; Fig. 3) via cofactors ($F_{420}H_2$) (Fig. 5D–E). Interpretation of these results are discussed further in 5.2.1.

Table 3. Isotope flux-balance model results for *Archaeoglobus fulgidus*.

Growth phase	Scenario		$f_{W,net}$ (%)[c]			$\varepsilon_{W,net}$ (‰)[d]			$\varepsilon_{S,net}$ (‰)[e]		
	x_{ex} (%)[a]	s (%)[b]	T-L	S-L	T-H	T-L	S-L	T-H	T-L	S-L	T-H
Exp.	0	0	41	41	100	179	167	–448	–511	–523	n/a
	0	100	31	31	80	561	546	–312	–582	–592	–564
	100	0	70	70	100	–312	–319	–448	–36	–59	n/a
	100	100	60	60	90	–198	–206	–387	–277	–294	–139
Sta.	0	0	41	41	100	341	270	–372	–636	–595	n/a
	0	100	31	31	80	776	682	–218	–688	–654	–785
	100	0	70	70	100	–218	–259	–372	–282	–201	n/a
	100	100	60	60	90	–87	–136	–302	–461	–401	–577

[a] the degree of water exchange during lipid synthesis, which depends on the extent of re-equilibration during isomerization steps (steps 2 and 6; Supporting Information, Fig. S1).
[b] the degree of H contribution to lipids from substrate (lactate for heterotrophy; H_2 for autotrophy)
[c] the net total contribution of H from water to lipids ($f_{W,net} = f_{W,direct} + f_{W,cofa}$)
[d] the net isotope fractionation between water and lipid (combining isotope effects associated with the water-derived fluxes, $f_{W,direct}$ and $f_{W,cofa\text{-}LS}$)
[e] the net isotope fractionation between substrate and lipid (combining isotope effects associated with the substrate-derived fluxes, $f_{S,cofa\text{-}LS}$ and $f_{S,AS}$)

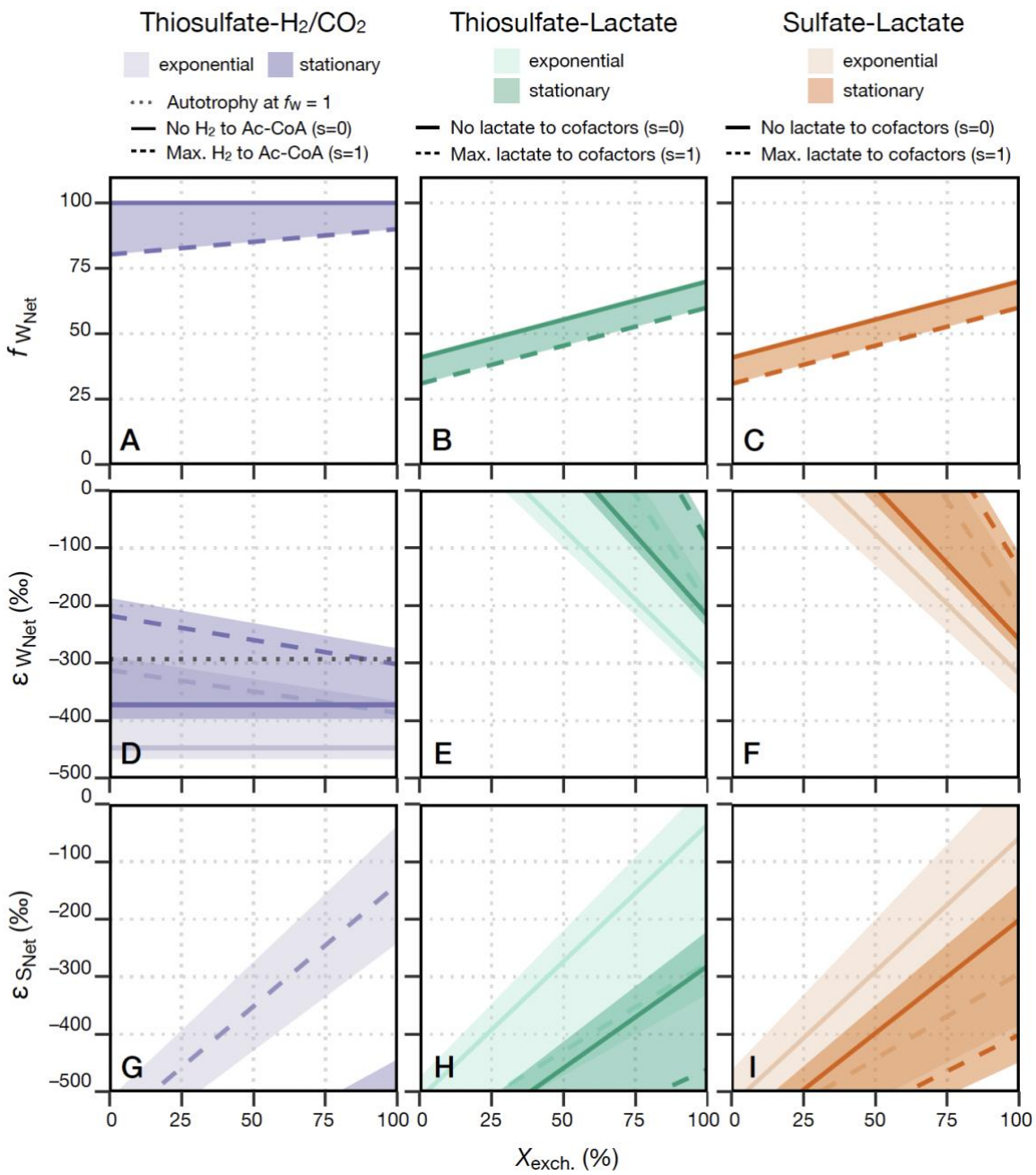

Figure 4. Isotope flux-balance model results for *Archaeoglobus fulgidus*. (A–C) Net fraction of total hydrogen derived from water ($f_{W,net}$); (D–F) Net isotope fractionation between lipid and water ($\varepsilon_{W,net}$); (G–I) Net isotope fractionation between lipid and substrate ($\varepsilon_{S,net}$). Each column represents the metabolic mode and growth substrates: heterotrophy on thiosulfate and lactate (A, D and G); heterotrophy on sulfate and lactate (B, E and H); and autotrophy on thiosulfate and H_2/CO_2 (C, F and I). Lighter shaded areas refer to exponential growth phase; darker shades refer to stationary growth phase. Solid lines refer to the s = 0 % (minimal substrate contribution) scenarios; dashed lines refer to the s = 100 % (maximal substrate contribution) scenarios. See 4.2.1 and Supporting Information Table S1 for details of the conditions for each scenario.

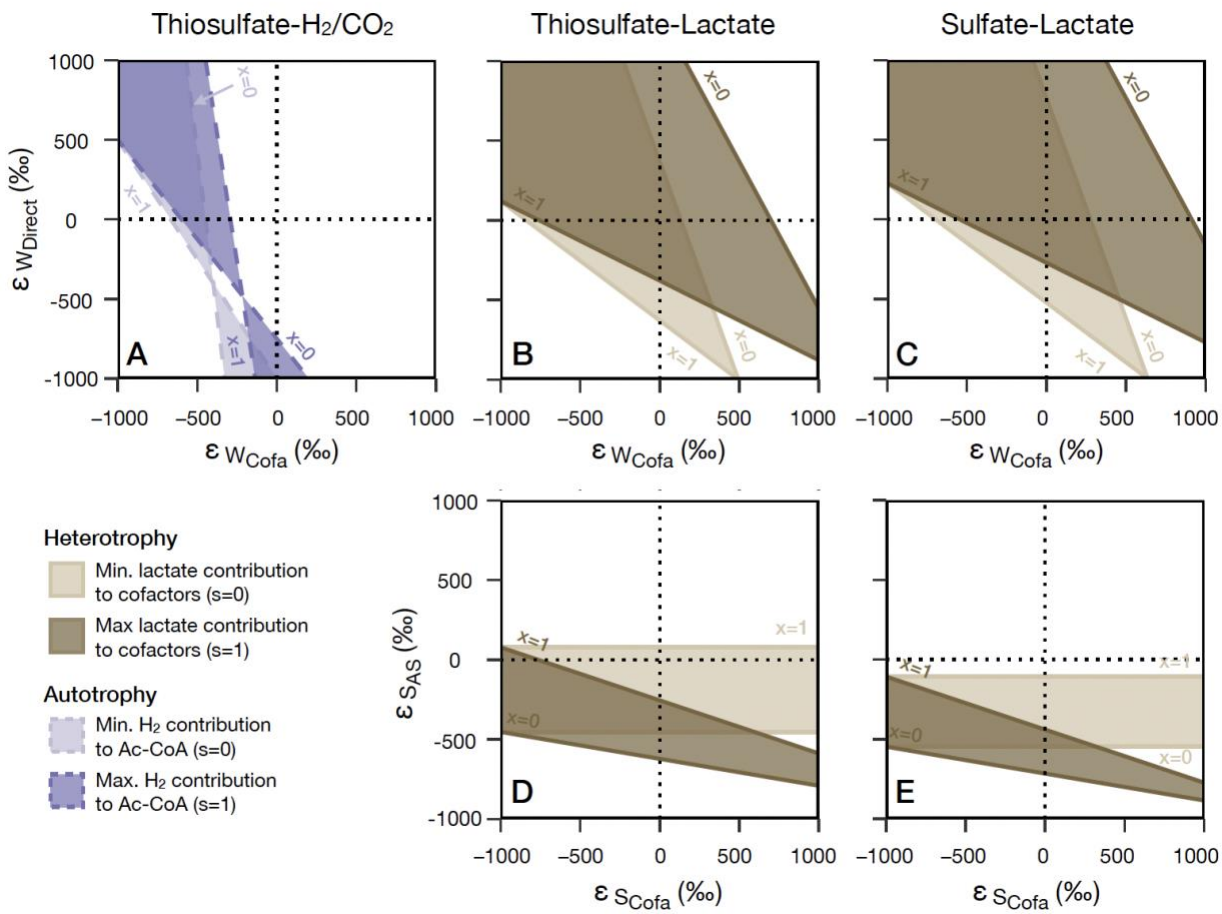

Figure 5. Isotope flux-balance model results for *Archaeoglobus fulgidus*. (A–C) Breakdown of the net isotope fractionation between lipid and water ($\varepsilon_{W,net}$; Fig. 4D–F) into two different isotope fractionation factors associated with water-derived H: $\varepsilon_{W,direct}$ for water-derived H atoms that are transferred through exchange during isomerization or addition via GGR, corresponding to $f_{W,direct}$ in Fig. 3, and $\varepsilon_{W,cofa}$ for water-derived H atoms that are transferred through cofactors (Fd_{red} and $F_{420}H_2$ for autotrophy, panel A; Fd_{red} for heterotrophy, panels B and C), corresponding to $f_{W,cofa}$ in Fig. 3. (D–E) Breakdown of the net isotope fractionation between lipid and substrate ($\varepsilon_{S,net}$; Fig. 4G–I) into two different isotope fractionation factors associated with substrate-derived H: $\varepsilon_{S,AS}$ for substrate-derived H atoms that are inherited directly from substrate via Ac-CoA, corresponding to $f_{S,AS}$ in Fig. 3, and $\varepsilon_{S,cofa}$ for substrate-derived H atoms that are transferred through cofactors (only applicable for heterotrophy via $F_{420}H_2$, panels D and E), corresponding to $f_{S,cofa}$ in Fig. 3. The lighter shaded areas refer to the s = 0 % (minimal substrate contribution) scenarios; darker shaded areas refer to the s = 100 % (maximal substrate contribution) scenarios. Solid lines and brown colors refer to heterotrophic conditions; dashed lines and purple colors refer to autotrophic conditions. See 4.2.1 and Supporting Information Table S1 for details of the conditions for each scenario.

5. Discussion

5.1. Effects of carbon metabolism and growth phase on lipid H isotope composition

Isotope flux-balance model results suggest that a large fraction of lipid-bound H in *A. fulgidus* is sourced from water. The fraction was larger for the autotrophic case ($f_{W,net}$ = 80–100 %); the $f_{W,net}$

range for the heterotrophic cases was relatively lower ($f_{W,net}$ = 31–70 %; Table 3; Fig. 4A–C). However, considering that $\varepsilon_{W,net}$ is most likely a negative value (i.e., a normal kinetic isotope fractionation), we can constrain the $f_{W,net}$ range that corresponds to $\varepsilon_{W,net} < 0$ in Fig. 4D–E. This yields the $f_{W,net}$ ranges of: 38–52 % for T-L and 42–52 % for S-L during exponential growth phase, versus 50–56 % for T-L and 52–54 % S-L during stationary growth phase. The lowest $f_{W,net}$ were therefore recorded during heterotrophy at exponential phase growth, independent of the terminal electron acceptor. Moreover, ≥80 % of lipid-bound H during autotrophy and ≥50 % of lipid-bound H in stationary phase cultures of *A. fulgidus* during heterotrophy originate from water. The $f_{W,net}$ range for lipids produced during stationary phase alone is likely even larger, because lipids collected during stationary phase are a mixture of those produced during exponential phase and those newly produced during stationary phase. The higher $f_{W,net}$ range observed for autotrophy is reasonable, given that lactate is an additional source of H that contributes directly to Ac-CoA synthesis during heterotrophy. A similar observation was reported for bacterial lipids where, for instance, the mole fraction of lipid H derived from water (≡ X_W in Zhang et al., 2009; herein equivalent to $f_{W,net}$) was larger for *Escherichia coli* grown on glucose compared to the same organism grown on complex medium (Zhang et al., 2009). Though the lipid synthesis pathways are different for Bacteria versus Archaea, it appears that the fractional contribution of water to lipid H generally decreases when substrates that are more direct precursors for lipid biosynthesis are used.

The effects of carbon metabolism and growth phase on lipid isotope composition have not been investigated in detail for archaeal lipids. Our results indicate that both the mode of metabolism and growth phase affect the lipid isotope composition (Table 3; Fig. 4). A recent study reported $\varepsilon_{L/W}$ of BPs produced by *N. maritimus* in continuous cultures at a range of doubling time and observed little change in $\varepsilon_{W/L}$ (0.18 ± 0.09 ‰ increase in $\varepsilon_{L/W}$ per hour increase in doubling time; Leavitt et al., 2023). The relative variation in doubling time we observe for *A. fulgidus* grown on different substrates here in batch cultures (Table 1) is comparable (*ca*. 3-fold variation) to the variation observed for *N. maritimus* in Leavitt et al. (2023). A key difference here is that we do not strictly control growth and metabolic rates, as was the case for chemostat cultivation of *N. maritimus* (Leavitt et al., 2023), and for *Sulfolobus acidocaldarius* (Harris et al., 2022). Nonetheless, the range of $\varepsilon_{L/W}$ we observe across different metabolic modes by *A. fulgidus* (–231 ± 6 ‰ for T-L, –241 ± 4 ‰ for S-L, and –271 ± 18 ‰ for T-H_2/CO_2; Table 2) is significant compared to the entire range of $\varepsilon_{L/W}$ observed across a comparable variation in growth rate by *N. maritimus* (–272 ± 20 to –279 ± 8 ‰ for BP-0; Leavitt et al., 2023). *N. maritimus* is an obligate chemoautotroph, such that all BP-bound H is strictly biosynthetic, whereas we show here that patterns of $\varepsilon_{W/L}$ can change between heterotrophic and autotrophic growth conditions (Fig. 4 and 6). Our results support this hypothesis and show variation in $\varepsilon_{L/W}$ up to ~40 ‰ within the same metabolically versatile organism, in response to different electron donor-acceptor pairs and modes of carbon metabolism.

Even though the range of $\varepsilon_{L/W}$ in *A. fulgidus* is relatively larger compared to *N. maritimus*, the overall variation of $\varepsilon_{L/W}$ across all archaeal lipid studies to-date is consistently small (Fig. 6).

5.2. Factors that affect $\varepsilon_{L/W}$ across the three domains of life

Here we present a synthesis of the broader $\varepsilon_{L/W}$ patterns observed in lipids from all three domains of life. Archaeal lipids are characterized by a relatively narrow range of depleted $\varepsilon_{L/W}$ across a wide range of organisms, metabolisms, and growth conditions (Fig. 6; Kaneko et al., 2011; Wu et al., 2020; Leavitt et al., 2023; this study). This is in contrast with the domain Bacteria, where fatty acid $\varepsilon_{L/W}$ ranges a large span of >600 ‰ with both highly enriched and depleted values (Fig. 6; Campbell et al., 2009; Zhang et al., 2009; Dawson et al., 2015; Osburn et al., 2016; Wijker et al., 2019). Archaeal lipid $\varepsilon_{L/W}$ largely overlaps with that of eukaryotic lipid $\varepsilon_{L/W}$, although eukaryotic lipid $\varepsilon_{L/W}$ spans a significant range depending on the types of organism and classes of compound (Fig. 6; Sessions et al., 1999; Chikaraishi et al., 2004, 2009; Zhang and Sachs, 2007; Sachs et al., 2016). Notably, there are subgroups of both domains Bacteria and Eukarya that share similarities with Archaea in their $\varepsilon_{L/W}$. The shared similarities are interesting, given the difference in lipid biosynthesis mechanism among the three domains. Below, we take a closer look at the specific subsets of $\varepsilon_{L/W}$ values from the domains Euakrya and Bacteria that resemble those from Archaea and discuss factors that may contribute to the depletion of $\varepsilon_{L/W}$ observed across the three domains.

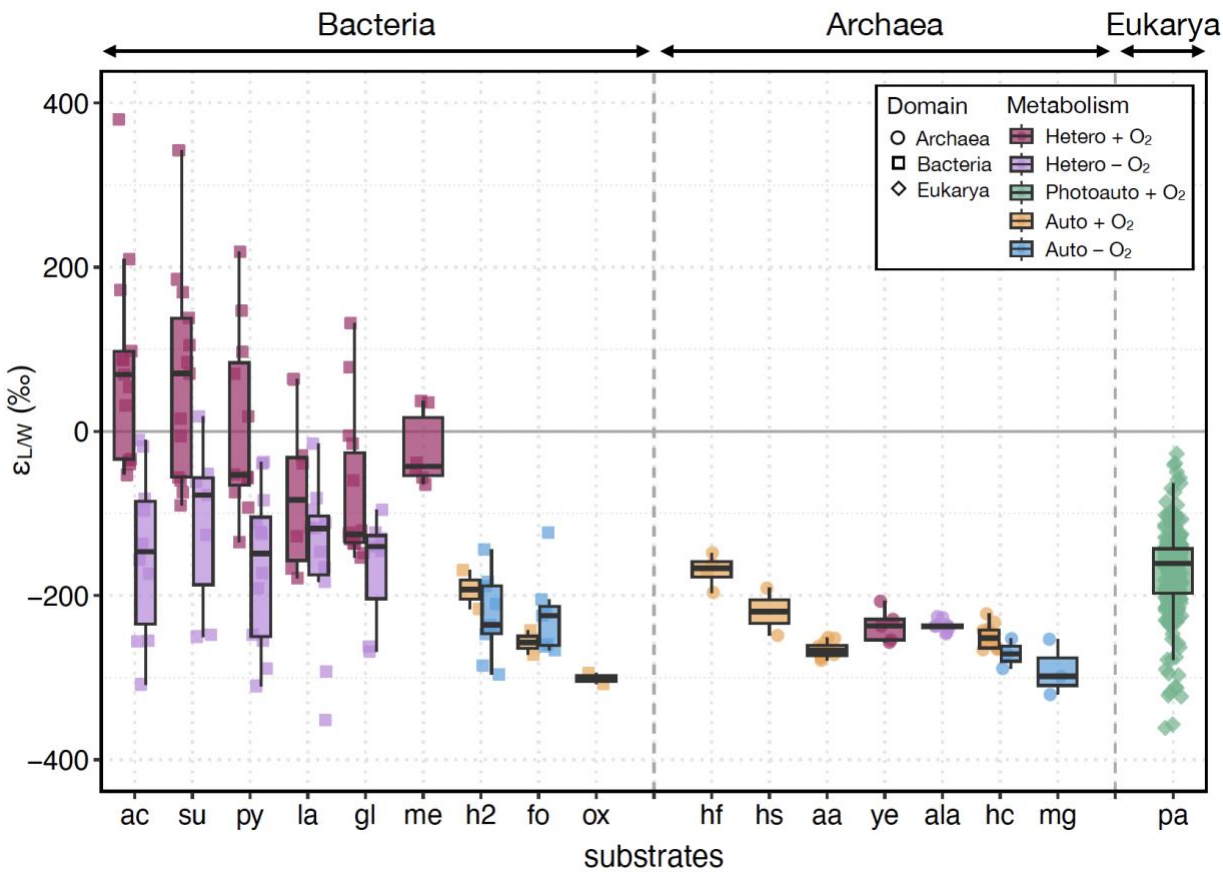

Figure 6. Summary of hydrogen isotope fractionation ($\varepsilon_{L/W}$) between lipids and water observed in culture studies. $\varepsilon_{L/W}$ values observed in all three domains of life: Archaea (circle), Bacteria (square), and Eukarya (diamond). Color codes represent different types of metabolism: aerobic heterotrophy (red), anaerobic heterotrophy (purple), aerobic photoautotrophy (green), aerobic chemoautotrophy (orange), and anaerobic chemoautotrophy (blue). Electron donors used for biosynthesis are shown on the horizontal axis: acetate (ac); succinate (su); pyruvate (py); lactate (la/ala); glucose (gl/agl); methane (me); H_2+CO_2 (h2/hc); formate (fo); oxalate (ox); H_2+Fe^{3+} (hf); H_2+S^0 (hs); ammonium (aa); yeast extract (ye); H_2, acetate or methanol for methanogenesis (mg); water for photoautotrophy (pa). Tested organisms for bacterial cultures include *C. oxalaticus*, *C. necator*, *R. palustris* (Zhang et al., 2009); *E. coli* (Zhang et al., 2009; Osburn et al., 2016; Wijker et al., 2019); *D. autotrophicum* (Campbell et al., 2009; Osburn et al., 2016); *M. capsulatus* (Sessions et al., 2002); *D. multivorans* (Dawson et al., 2015); *D. alaskensis* (Leavitt et al., 2016); *P. denitrificans, S. oneidensis, D. hydrogenophilus, D. alaskensis, D. propionicus* (Osburn et al., 2016); *B. subtilis, P. fluorescens, R. radiobacter, and E. meliloti* (Wijker et al., 2019). Tested organisms for eukaryotic cultures include *A. fundyense, I. galbana, Ascophyllum sp., F. vesiculosis, Z. marina, S. alterniflora* (Sessions et al., 1999); *C. japonica* (Chikaraishi, Naraoka and Poulton, 2004); *B. braunii, E. unicocca, V. aureus* (Zhang and Sachs, 2007); *C. sativuc* (Chikaraishi et al., 2009); *E. huxleyi* (Sachs et al., 2016). Tested organisms for archaeal cultures include *Acidianus* sp. DS80 ('hf' and 'hs', this study); *N. maritimus* ('aa', Leavitt, Kopf et al., 2023); *Sulfolobus* sp. ('ye', Kaneko et al., 2011); *A. fulgidus* ('ala' and 'hc', this study); *Metallosphaera sedula* ('hc',this study); and *M. barkeri* ('mg', Wu et al., 2020).

5.2.1. Large $\varepsilon_{L/W}$ associated with isoprenoid saturation: Archaeal and Eukaryotic lipids

The consistently depleted values of $\varepsilon_{W/L}$ for archaeal lipids are notable considering the different types of organism and metabolic modes studied so far (Fig. 6). In Fig. 5, we present the model solution spaces for individual H fluxes, within either net water-derived flux ($f_{W,net}$) or net substrate-derived flux ($f_{S,net}$), to further investigate specific parts of archaeal lipid biosynthesis pathway that may contribute to the observed depletion of bulk $\varepsilon_{L/W}$. Prior work yielded estimates of $\alpha_W \cong 0.9$ for isotope fractionation associated with direct water incorporation across many bacteria (Zhang et al., 2009; Wijker et al., 2019), and $\varepsilon_{L/W}$ values modeled for *N. maritimus* with this empirical α_W were consistent with experimental observations (Leavitt et al., 2023). Assuming an equivalent value of $\varepsilon_{W,direct}$ (i.e., isotope fractionation associated with the $f_{W,direct}$ flux is –100 ‰), we constrain plausible ranges of $\varepsilon_{W,cofa}$ (water-derived H fluxes that involve Fd_{red} and $F_{420}H_2$) in *A. fulgidus* (Fig. 5A–C). The ranges of $\varepsilon_{W,cofa}$ at $\varepsilon_{W,direct}$ = –100 ‰ are particularly well constrained for the autotrophic case (–599 to –436 ‰ at s = 0 %; –519 to –276 ‰ at s = 100 %; Fig. 5A).

It is plausible that both $\varepsilon_{W,cofa\text{-}AS}$ and $\varepsilon_{W,cofa\text{-}LS}$ have negative values that are comparable to the combined value of $\varepsilon_{W,cofa}$, as the less likely alternative would be a negative $\varepsilon_{W,cofa}$ that consists of very different $\varepsilon_{W,cofa\text{-}AS}$ and $\varepsilon_{W,cofa\text{-}LS}$. Our current model cannot distinguish between isotope fractionation factors associated with different fluxes within $f_{W,cofa}$ (i.e., $f_{W,cofa\text{-}AS}$ through Ac-CoA *vs*. $f_{W,cofa\text{-}LS}$ through NADPH), both of which can inherit water-derived H from cofactors $F_{420}H_2$ and/or Fd_{red} (Fig. 3B). However it is worth noting that, for both heterotrophic and autotrophic cases, a fraction of the $f_{W,cofa\text{-}LS}$ flux represents hydride transfer during the final saturation (double bond reduction) via GGR (Fig. 3; step 10, Fig., S1). Results of the isotope flux-balance model for *N. maritimus* also indicated that the GGR reduction step is strongly fractionating (ε_{GGR} = –690 to –820 ‰ if ε_{NADPH} = –100 to –300 ‰, depending on the degree of water exchange, or x_{ex} in this study), regardless of how other model parameters are set (Leavitt et al., 2023). Given how *N. maritimus* and *A. fulgidus* share little in common otherwise (metabolically, genetically, and biochemically), large fractionation associated with the GGR reduction step provides a parsimonious explanation for the similar $\varepsilon_{L/W}$ values observed in the two organisms, as it is the final step of archaeal lipid biosynthesis shared across all tetraether-producing Archaea. This would be consistent with the similarly depleted $\varepsilon_{L/W}$ values observed in other archaeal lipids (Fig. 6); testing more Archaea with the combined approach of isotope labeling experiments and biochemically informed isotope flux-balance model will help further confirm this idea.

A closer examination of the eukaryotic lipids that shares similar $\varepsilon_{L/W}$ values to archaeal lipids lends further support to the notion that GGR reduction contributes to large H isotope fractionation between lipids and water. Fig. 7A shows $\varepsilon_{L/W}$ for different subgroups of eukaryotic lipids, categorized by three different biosynthetic pathways. In general, the two major families of lipids are acetogenic and isoprenoid lipids which consist of acetate and isoprene monomeric units, respectively (Pearson, 2014). Isoprenoid lipids are further divided into two groups, depending on whether the isoprene (C_5) building blocks are synthesized via the mevalonic acid (MVA) pathway (Lynen et al., 1958; Bloch, 1959) or the methylerythritol phosphate (MEP) pathway (Rohmer et

al., 1993). All Archaea discussed in this study synthesize isoprenoid lipids via the MVA pathway. The MEP pathway is generally defined as bacterial and the MVA pathway as eukaryotic and archaeal; both pathways often simultaneously occur in plants, where the MEP pathway is expressed in chloroplasts (relics of the cyonobacterial plastid ancestor) and the MVA pathway is expressed in the cytosol (Lichtenthaler et al., 1997; Lichtenthaler, 1999; Pearson, 2014). An exception to this is the case of green algae, where both the cytosolic sterols and plastidic phytol isoprenoids are synthesized via the MEP pathway (Schwender et al., 1996; Disch et al., 1998; Pearson, 2014).

For eukaryotic lipids, it has been recognized for several decades that the three different biosynthetic pathways (acetogenic, MVA, and MEP) are associated with distinct ranges of $\varepsilon_{L/W}$. In general, isoprenoid lipids have more negative $\varepsilon_{L/W}$ compared to acetogenic lipids (Estep and Hoering, 1980; Sessions et al., 1999). Among isoprenoid lipids, plastidic isoprenoids such as phytols are more depleted than the cytosolic counterparts (Sessions et al., 1999; Chikaraishi et al., 2004, 2009). This general trend is captured in Fig. 7A, where acetogenic lipids (e.g., *n*-alkanol and *n*-alkyl lipids including fatty acids) have more positive $\varepsilon_{L/W}$ compared to isoprenoid lipids. The C_{15} and C_{30} isoprenoids synthesized via the MVA pathway (e.g., sterol, triterpenoids, sesquiterpenes, squalene) are relatively more enriched in ^{2}H compared to the C_{20} isoprenoids (e.g., phytol, phytadiene, diterpenes) and botryococcenes (triterpenes) synthesized via the MEP pathway (Fig. 7A).

While the relative difference in $\varepsilon_{L/W}$ between MVA and MEP pathways holds in general, the degree of extreme depletion in $\varepsilon_{L/W}$ appears to correlate more with highly fractionating enzymatic steps, rather than specific pathways. For example, Chikaraishi et al. (2004) observed in *Cryptomeria japonica* (conifer) that $\varepsilon_{L/W}$ values for cytosolic lipids produced via the MVA pathway, sesquiterpenes (–228 to –238 ‰) and squalene (–225 to –251 ‰), are comparable to those for plastidic diterpenoids (–238 to –251 ‰) produced via the MEP pathway (Fig. 7A). Phytol and botryococcenes, on the other hand, have particularly depleted $\varepsilon_{L/W}$ values among eukaryotic lipids produced via the MEP pathway. For example, Zhang and Sachs (2007) found that botryococcenes with longer chain lengths had progressively lower δ^2H compared to the C_{30} botryococcene (precursor to all other botryococcenes) in *Botryococcus braunii* race B. They hypothesized that significantly ^{2}H-depleted hydrogen from methionine is incorporated into botryococcene during the step-wise methylation (Zhang and Sachs, 2007). Similarly, phytol in *C. japonica* had up to 65 ‰ more negative $\varepsilon_{L/W}$ compared to diterpenoids, another plastidic lipid produced via the MEP pathway within the same organism (Chikaraishi et al., 2004). Later, Chikaraishi et al. (2009) observed a gradual depletion in δ^2H from phytol precursors (starting from geranylgeraniol) to phytol in cucumber, indicating that significantly ^{2}H-depleted hydrogen is incorporated into phytol and its precursors during the step-wise hydrogenation catalyzed by GGR ($\varepsilon_{GGR} \cong$ –650 ‰; Chikaraishi et al., 2009).

The $\varepsilon_{L/W}$ values of phytol (and its dehydration product phytadiene) investigated in a wide range of eukaryotes so far are all significantly depleted (e.g., –278 to –357 ‰ for phytol in dinoflagellate, coccolithophore, marsh grass, cucumber, and conifer; Fig. 7A). Similarly, all values of $\varepsilon_{L/W}$ investigated in a range of different archaea are significantly depleted (e.g., –341 to –148 ‰ for phytanes and biphytanes in *N. maritimus*, *Sulfolobus* sp., *M. sedula*, *Acidianus* sp., *M. barkeri*, and *A. fulgidus*; Fig. 7A). Taken together, empirical and model-based results suggest that the GGR reduction is a highly fractionating step that contribute to the large fractionation observed in both eukaryotic and archaeal lipid synthesis (Chikaraishi et al., 2009; Leavitt et al., 2023; this study; Fig. 5 and 6).

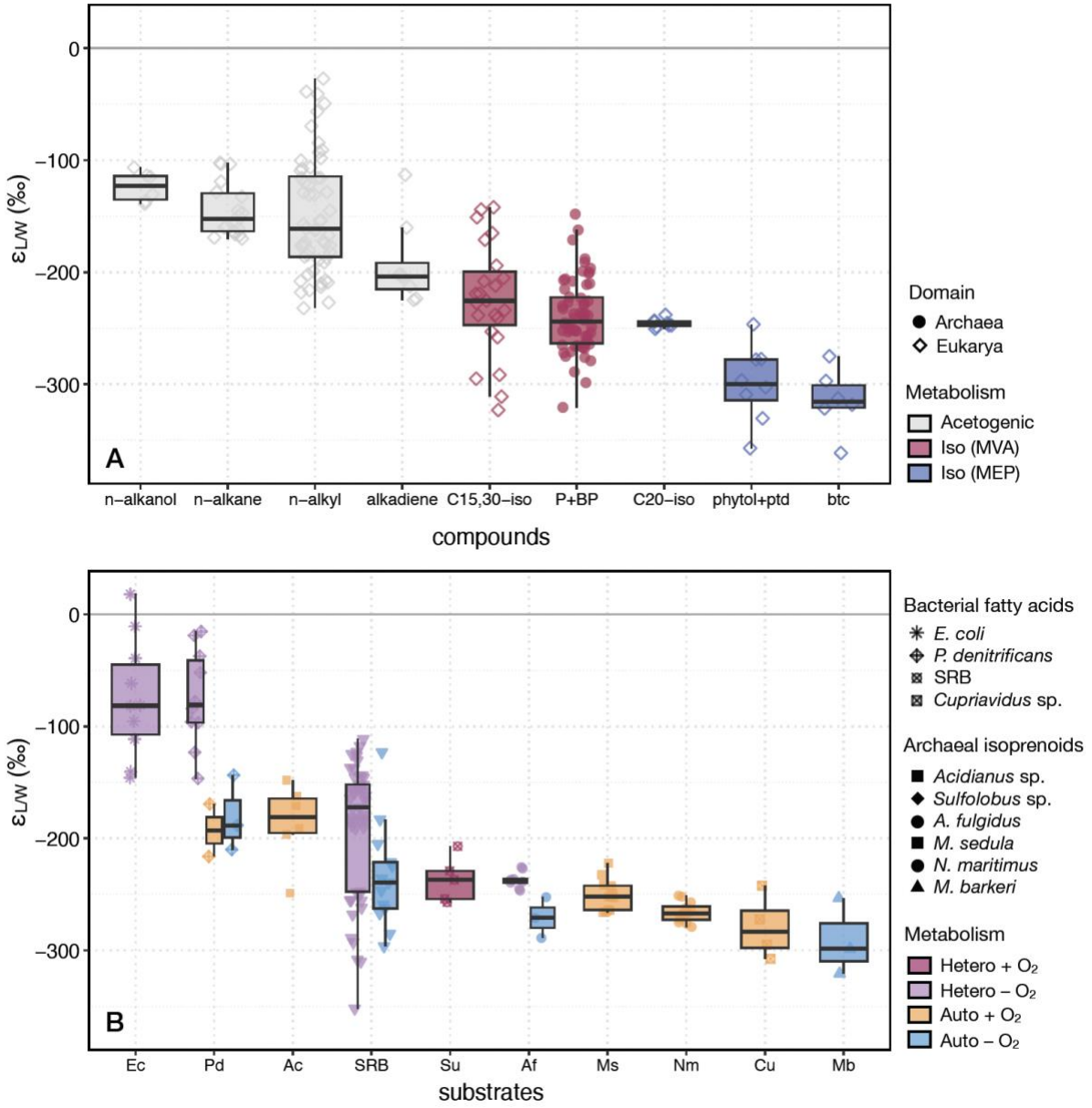

Figure 7. Comparison of $\varepsilon_{L/W}$ values observed in eukaryotic *vs*. archaeal lipids and in bacterial *vs*. archaeal lipids. **(A)** $\varepsilon_{L/W}$ values observed in acetogenic and isoprenoid lipids from the domains Archaea and Eukarya. Different classes of compounds are shown on the horizontal axis. Compounds shown for acidogenic pathway: n-alkanol, *n*-alkane, *n*-alkyl (*n*-alkanoic acids and fatty acids), and alkadiene. For the MVA pathway: C_{15} and C_{30} isoprenoids (sterol, squalene, triterpenoids, and sesquiterpenes) and P+BP (phytanes and biphytanes). For the MEP pathway: C_{20} isoprenoids (diterpenes, sandaracopimarinol, ferruginol, diterpenol, and sugiol), phytol+ptd (phytol and phytadiene), and btc (botryococcene). **(B)** $\varepsilon_{L/W}$ values observed in fatty acids from anaerobic and/or autotrophic Bacteria and isoprenoid lipids from Archaea. Different organisms are shown on the horizontal axis. For Bacteria: *E. coli* (Ec), *Paracoccus denitrificans* (Pd), SRB (*Desulfobacterium autotrophicum*, *Desulfococcus multivorans*, *Desulfobacter hydrogenophilus*, *Desulfovibrio alaskensis*, *Desulfolobus propionicus*), and *Cupriavidus* sp. (Cu). For Archaea: *Acidianus* sp. DS80 (Ac), *Sulfolobus* sp. (Su), *Archaeoglobus fulgidus* (Af), *Metallosphaera sedula* (Ms), *Nitrosopumilus maritimus* (Nm), and *Methanosarcina barkeri* (Mb). A full list of references can be found in Supporting Information.

5.2.2. Effect of energy limitation on $\varepsilon_{W/L}$: Archaeal and Bacterial lipids

Besides the shared biochemical mechanism underlying negative $\varepsilon_{L/W}$ in eukaryotic and archaeal lipids, another interesting pattern emerges from comparison of $\varepsilon_{L/W}$ across the three domains of life: a subset of bacterial lipids resembles archaeal lipids in its consistently negative $\varepsilon_{L/W}$ values (Fig. 6). For bacterial lipids, anaerobiosis and/or autotrophy appear to be associated with consistently depleted ranges of $\varepsilon_{L/W}$. Examples include aerobic autotrophy (*Cupriavidus oxalaticus*, Zhang et al., 2009; *Paracoccus denitrificans*, Osburn et al., 2016), anaerobic autotrophy (*Desulfobacterium autotrophicum*, Campbell et al., 2009; *Desulfococcus multivorans*, Dawson et al., 2015; *P. denitrificans*, *Desulfobacterium autotrophicum*, *Desulfovibrio alaskensis*, Osburn et al., 2016), and anaerobic heterotrophy (*D. multivorans*, Dawson et al., 2015; *P. denitrificans*, *Escherichia coli*, *D. autotrophicum*, *Desulfobacter hydrogenophilus*, *D. alaskensis*, *Desulfolobus propionicus*, Osburn et al., 2016) (Fig. 6; Fig. 7B). Of these modes of metabolism, aerobic or anaerobic autotrophy has a more constrained range of $\varepsilon_{W/L}$ and more overlaps with the depleted $\varepsilon_{L/W}$ observed in archaeal lipids, compared to anaerobic heterotrophy (Fig. 6; Fig. 7B). We propose that NADPH flux imbalances associated with energy limitation that broadly characterize autotrophic and/or anaerobic modes of metabolism contribute to the apparent similarity in $\varepsilon_{L/W}$ observed between the domains of Bacteria and Archaea.

The concept of NADPH flux imbalance set forth by Wijker et al. (2019) provides a quantitative framework to relate metabolism-dependent patterns of $\varepsilon_{L/W}$ observed in aerobic heterotrophs to the fluxes of H through specific dehydrogenase and transhydrogenase enzymes. For the highly conserved fatty acid biosynthesis pathway, NADPH serves as the reducing agent for the reduction of acyl intermediates (Wakil et al., 1983). As a result, NADPH accounts for ~50% of fatty acid H (Sessions et al., 1999). Wijker et al. (2019) showed that $\varepsilon_{L/W}$ values of fatty acids produced by five wild-type species of aerobic heterotrophic bacteria are positively correlated with relative NADPH imbalance flux. Among the tested aerobic heterotrophs, two species (*E. coli* and *B. subtilis*) had

moderately negative values of NADPH flux imbalance (–32 and –11 %, respectively) (Wijker et al., 2019). Here, negative values reflect underproduction of NADPH where catabolic production of NADPH does not meet the anabolic requirement (Wijker et al., 2019). Furthermore, the results from *E. coli* knockout mutants confirmed the direction of isotope fractionation for specific transhydrogenases (e.g., ^{2}H-depletion by NADPH-producing PntAB and ^{2}H-enrichment by NADPH-consuming UDhA) (Wijker et al., 2019).

For microbes adapted to chronic energy limitation, even more negative values of NADPH flux imbalance would be expected where just enough NADPH is produced such that most to all of it is used for biosynthesis (i.e., little to no flux from NADPH back to NADH). This prediction is consistent with the general concept of energy spilling (also known as growth uncoupling or overflow metabolism), which suggests that microbes under energy limitation tend to have more efficient biomass production (Russell, 2007). For example, *E. coli* grown aerobically resulted in more than 9-fold increase in ATP production per mole of glucose compared to the anaerobic counterpart; however, the biomass yield was only 2-fold greater during aerobic respiration (Stouthamer and Bettenhaussen, 1977; Gottschalk, 1986). Similar phenomenon of energy spilling has also been observed in methanogenic archaea. For example, *Methanothermobacter thermautotrophicus* and *Methanococcus maripaludis* produced less cells per mole of methane when H_2 (electron donor) was present in excess compared to H_2-limiting condition (Morgan et al., 1997; De Poorter et al., 2007; Costa et al., 2013).

In line with the observed and expected outcomes of energy limitation (negative NADPH flux imbalance and tighter coupling between catabolism and anabolism), Leavitt et al. (2023) found that $\varepsilon_{L/W}$ values for *N. maritimus* fall within the 95% confidence interval for the extension of Wijker et al. (2019) regression when an extremely negative value (–100 %) of NADPH flux imbalance was assigned. The apparent fit of *N. maritimus* $\varepsilon_{L/W}$ on the negative end of the framework is reasonable, given that *N. maritimus* is an obligate autotroph adapted to oligotrophic nitrification with energy-efficient CO_2 fixation pathway (Martens-Habbena et al., 2009; Könneke et al., 2014). The fact that all archaeal lipids investigated for $\varepsilon_{L/W}$ so far fall within a relatively narrow range of negative values (Fig. 6; Fig. 7B) may, at least partially, reflect the general concept that Archaea are optimized for chronic energy limitation (Valentine, 2007). The results from this study show that, while metabolic modes and growth rates have significant impacts on $\varepsilon_{L/W}$ within a single organism (*A. fulgidus*), the observed variation in $\varepsilon_{L/W}$ still falls within the overall range observed across archaeal lipids (e.g., heterotrophic and autotrophic *A. fulgidus* 'Af' data *vs*. other archaeal lipids data; Fig. 7B).

The similarity between archaeal lipids and a subset of anaerobic and/or autotrophic bacterial lipids is striking (Fig. 6; Fig. 7B) given the fundamental differences in fatty acid and isoprenoid lipid biosynthesis pathways. This suggests that factors controlling microbial $\varepsilon_{L/W}$ may not be domain-specific; instead, common challenges associated with anaerobic respiration and/or autotrophy (i.e.,

lower free energy yields and/or additional energetic costs for CO_2 fixation) may become primary controlling factors of $\varepsilon_{L/W}$ for both Bacteria and Archaea. Notably, the range of $\varepsilon_{L/W}$ in fatty acids produced by sulfate-reducing bacteria (SRB) is much narrower compared to that observed in aerobic heterotrophs regardless of metabolic pathway or substrate (Fig. 7B).

One of the transhydrogenases that plays an important role in SRB is NfnAB, and it has been shown that this enzyme is important for H isotope fractionation in *D. alaskensis* (Leavitt et al., 2016). The details of the magnitude of $\varepsilon_{L/W}$ set by NfnAB under severe NADPH underproduction may be complicated by other processes such as intracellular isotope distillation (i.e., more quantitative transfer of NADPH hydride to lipids) as suggested by Leavitt et al. (2016). Regardless, given that decoupling of NADPH production for anabolism from NADH for catabolism becomes more important during energy limitation, transhydrogenases that are widely distributed among anaerobic bacteria (namely NfnAB; Pereira et al., 2011; Leavitt et al., 2016; Buckel and Thauer, 2018) may be key contributing factors for the negative $\varepsilon_{W/L}$ observed across these organisms (Fig. 6; Fig. 7B). It is worth noting that *nfnAB* was not found in archaeal species investigated by Pereira et al. (2011), including *A. fulgidus*.

A complex interplay among environmental, physiological, and enzymatic factors underlie net isotope fractionation patterns observed in a biosynthetic product such as $\varepsilon_{L/W}$. For archaeal lipids and a subset of bacterial lipids, however, two factors appear to play key roles in shaping the consistently negative $\varepsilon_{L/W}$ patterns observed in the lipids from both domains: highly fractionating enzymatic steps (e.g., GGR in archaeal isoprenoid lipid biosynthesis; transhydrogenases in bacterial fatty acid biosynthesis) and energy limitation (i.e., NADPH flux imbalance). The negative $\varepsilon_{L/W}$ commonly observed in archaea and a subset of bacteria is likely a convergent feature resulting from a combination of both factors. A better mechanistic understanding of factors conducive to similar patterns of $\varepsilon_{L/W}$ in bacterial and archaeal lipids could lead to biogeochemical and/or ecological insights that are unique to microbial life. This would, in turn, significantly expand the application of lipid biomarkers as paleoenvironmental or paleoecological proxy currently possible with eukaryotic or bacterial lipids alone.

6. Conclusion

In this study, we conducted water isotope label experiments with a metabolically flexible and well-studied model archaeon *A. fulgidus* and quantified the hydrogen isotope fractionation between lipids and water in response to different carbon substrates and electron donor-acceptor pairs. We observed changes in regression parameters among experimental conditions, where higher slopes ($f_W \cdot {}^2\alpha_{L/W}$) were observed in autotrophic compared to heterotrophic conditions and during stationary compared to exponential growth phase. The bio-isotopic model further constrains individual parameters such as fractional contribution of water to lipids (f_W) and isotope fractionation between lipids and water ($\varepsilon_{L/W}$) that together make up the slope. These results are consistent with observations from regression parameters, where f_W is larger under autotrophic

condition and during stationary growth phase compared to the heterotrophic conditions and exponential growth phase. The model results also allow us to constrain plausible ranges of isotope fractionation associated with a specific route of hydrogen flux (e.g., flux for direct water incorporation *vs*. flux from water through cofactors). The model results point toward the isotope fractionation associated with the $f_{W,cofa}$ flux, which includes the hydride transfer during the final saturation via GGR, as a highly fractionating step. This is consistent with recent bio-isotopic model results for another archaeon *N. maritimus*. Finally, we synthesized a three-domain comparison of $\varepsilon_{L/W}$ patterns which suggests that the highly fractionating double bond reduction via GGR may also explain the similar magnitudes of depleted $\varepsilon_{L/W}$ observed between eukaryotic and archaeal lipids. Furthermore, the shared negative $\varepsilon_{L/W}$ values between fatty acids in anaerobic and/or autotrophic bacteria and isoprenoids in archaea may be associated with the general state of energy limitation experienced by the different groups of organisms. Additional experimental work with archaea that use carbon metabolism pathways that have not been examined with the bio-isotopic model (i.e., 3HP/4HB and reductive Wood-Ljungdahl pathways) as well as more systematic comparisons between bacterial and archaeal lipids will help determine the scope of applicability for microbial lipid $\varepsilon_{L/W}$ in paleoenvironmental and paleoecological studies.

7. Acknowledgements

This research was supported by funding from: collaborative research grant NSF EAR #1928303 (WDL, SHK); the American Chemical Society PRF #57209-DNI2 (WDL, YW); Simons Foundation Award #623881 (WDL); Swiss National Science Foundation P2BSP2_168716 (YW); NSF OCE-1843285 and 1702262 (AP). JHR was supported by the Dartmouth College Society of Fellows. We thank Ashley Maloney (CU Boulder), Felix Elling (then at Harvard), and Beverly Chiu (then at Dartmouth) for expert laboratory assistance.

8. References

Bender A. L. D. Genetic and Biological Studies on Solanum Plants: Insights into the Leaf Wax Alkane Paleoclimate Proxy.

Bloch K. (1959) Biogenesis and transformations of squalene. In *Biosynthesis of Terpenes and Sterols* Little, Brown and Company.

Brock T. D., Brock K. M., Belly R. T. and Weiss R. L. (1972) Sulfolobus: A new genus of sulfur-oxidizing bacteria living at low pH and high temperature. *Arch. F*[illegible]*r Mikrobiol.* **84**, 54–68.

Buckel W. and Thauer R. K. (2018) Flavin-Based Electron Bifurcation, Ferredoxin, Flavodoxin, and Anaerobic Respiration With Protons (Ech) or NAD+ (Rnf) as Electron Acceptors: A Historical Review. *Front. Microbiol.* **9**, 401.

Campbell B. J., Li C., Sessions A. L. and Valentine D. L. (2009) Hydrogen isotopic fractionation in lipid biosynthesis by H2-consuming Desulfobacterium autotrophicum. *Geochim. Cosmochim. Acta* **73**, 2744–2757.

Chikaraishi Y. and Naraoka H. (2003) Compound-specific δD–δ13C analyses of n-alkanes extracted from terrestrial and aquatic plants. *Phytochemistry* **63**, 361–371.

Chikaraishi Y., Naraoka H. and Poulson S. R. (2004) Carbon and hydrogen isotopic fractionation during lipid biosynthesis in a higher plant (Cryptomeria japonica). *Phytochemistry* **65**, 323–330.

Chikaraishi Y., Tanaka R., Tanaka A. and Ohkouchi N. (2009) Fractionation of hydrogen isotopes during phytol biosynthesis. *Org. Geochem.* **40**, 569–573.

Costa K. C., Yoon S. H., Pan M., Burn J. A., Baliga N. S. and Leigh J. A. (2013) Effects of H_2 and Formate on Growth Yield and Regulation of Methanogenesis in Methanococcus maripaludis. *J. Bacteriol.* **195**, 1456–1462.

Dawson K. S., Osburn M. R., Sessions A. L. and Orphan V. J. (2015) Metabolic associations with archaea drive shifts in hydrogen isotope fractionation in sulfate-reducing bacterial lipids in cocultures and methane seeps. *Geobiology* **13**, 462–477.

De Poorter L. M. I., Geerts W. J. and Keltjens J. T. (2007) Coupling of *Methanothermobacter thermautotrophicus* Methane Formation and Growth in Fed-Batch and Continuous Cultures under Different H_2 Gassing Regimens. *Appl. Environ. Microbiol.* **73**, 740–749.

Dirghangi S. S. and Pagani M. (2013) Hydrogen isotope fractionation during lipid biosynthesis by Haloarcula marismortui. *Geochim. Cosmochim. Acta* **119**, 381–390.

Disch A., Schwender J., Müller C., Lichtenthaler H. K. and Rohmer M. (1998) Distribution of the mevalonate and glyceraldehyde phosphate/pyruvate pathways for isoprenoid biosynthesis in unicellular algae and the cyanobacterium Synechocystis PCC 6714. *Biochem. J.* **333**, 381–388.

Estep M. F. and Hoering T. C. (1980) Biogeochemistry of the stable hydrogen isotopes. *Geochim. Cosmochim. Acta* **44**, 1197–1206.

Gottschalk (1986) Regulation of Bacterial Metabolism.

Harris C., Rhim J., Zhang Y., Cobban A., McFarlin J., Batther H., Kopf S. and Leavitt W. (2022) Determining controls on hydrogen isotope fractionation in archaeal tetraether lipids in a thermoacidophilic archaeal heterotroph. In *Goldschmidt2022 abstracts* Goldschmidt2022. European Association of Geochemistry, Honolulu, HI, USA.

Hayes J. M. (2001) Fractionation of the Isotopes of Carbon and Hydrogen in Biosynthetic Processes. *Stable Isot. Geochem.*, 225–277.

Hendrickson E. L. and Leigh J. A. (2008) Roles of Coenzyme F_{420}-Reducing Hydrogenases and Hydrogen- and F_{420}-Dependent Methylenetetrahydromethanopterin Dehydrogenases in Reduction of F_{420} and Production of Hydrogen during Methanogenesis. *J. Bacteriol.* **190**, 4818–4821.

Hocking W. P., Stokke R., Roalkvam I. and Steen I. H. (2014) Identification of key components in the energy metabolism of the hyperthermophilic sulfate-reducing archaeon Archaeoglobus fulgidus by transcriptome analyses. *Front. Microbiol.* **5**.

Kaneko M., Kitajima F. and Naraoka H. (2011) Stable hydrogen isotope measurement of archaeal ether-bound hydrocarbons. *Org. Geochem.* **42**, 166–172.

Klein A. R., Breitung J., Linger D., Stetter K. O. and Thauer R. K. (1993) extremely thermophilic sulfate reducing Archaeoglobusfulgidus: comparison of its properties with those of the cyclohydrolase from the extremely thermophilic Methanopyrus kandleri.

Könneke M., Schubert D. M., Brown P. C., Hügler M., Standfest S., Schwander T., Schada Von Borzyskowski L., Erb T. J., Stahl D. A. and Berg I. A. (2014) Ammonia-oxidizing archaea use the most energy-efficient aerobic pathway for CO_2 fixation. *Proc. Natl. Acad. Sci.* **111**, 8239–8244.

Kopec B. G., Feng X., Posmentier E. S. and Sonder L. J. (2019) Seasonal Deuterium Excess Variations of Precipitation at Summit, Greenland, and their Climatological Significance. *J. Geophys. Res. Atmospheres* **124**, 72–91.

Kunow J., Schwörer B., Stetter K. O. and Thauer R. K. (1993) A F420-dependent NADP reductase in the extremely thermophilie sulfate-reducing Archaeoglobusfulgidus.

Ladd S. N. and Sachs J. P. (2017) 2H/1H fractionation in lipids of the mangrove Bruguiera gymnorhiza increases with salinity in marine lakes of Palau. *Geochim. Cosmochim. Acta* **204**, 300–312.

Lai D., Springstead J. R. and Monbouquette H. G. (2008) Effect of growth temperature on ether lipid biochemistry in Archaeoglobus fulgidus. *Extremophiles* **12**, 271–278.

Leavitt W. D., Kopf S. H., Weber Y., Chiu B., McFarlin J. M., Elling F. J., Hoeft-McCann S. and Pearson A. (2023) Controls on the hydrogen isotope composition of tetraether lipids in an autotrophic ammonia-oxidizing marine archaeon. *Geochim. Cosmochim. Acta* **352**, 194–210.

Leavitt W. D., Venceslau S. S., Pereira I. A. C., Johnston D. T. and Bradley A. S. (2016) Fractionation of sulfur and hydrogen isotopes in *Desulfovibrio vulgaris* with perturbed DsrC expression ed. R. Boden. *FEMS Microbiol. Lett.* **363**, fnw226.

Lengger S. K., Weber Y., Taylor K. W. R., Kopf S. H., Berstan R., Bull I. D., Mayser J., Leavitt W. D., Blewett J., Pearson A. and Pancost R. D. (2021) Determination of the δ^2H values of high molecular weight lipids by high-temperature gas chromatography coupled to isotope ratio mass spectrometry. *Rapid Commun. Mass Spectrom.* **35**, e8983.

Lichtenthaler H. K. (1999) THE 1-DEOXY-D-XYLULOSE-5-PHOSPHATE PATHWAY OF ISOPRENOID BIOSYNTHESIS IN PLANTS. *Annu. Rev. Plant Physiol. Plant Mol. Biol.* **50**, 47–65.

Lichtenthaler H. K., Rohmer M. and Schwender J. (1997) Two independent biochemical pathways for isopentenyl diphosphate and isoprenoid biosynthesis in higher plants. *Physiol. Plant.* **101**, 643–652.

Lynen F., Eggerer H., Henning U. and Kessel I. (1958) Farnesyl-pyrophosphat und 3-Methyl-Δ^{3}-butenyl-1-pyrophosphat, die biologischen Vorstufen des Squalens. Zur Biosynthese der Terpene, III. *Angew. Chem.* **70**, 738–742.

Maloney A. E., Shinneman A. L. C., Hemeon K. and Sachs J. P. (2016) Exploring lipid 2H/1H fractionation mechanisms in response to salinity with continuous cultures of the diatom Thalassiosira pseudonana. *Org. Geochem.* **101**, 154–165.

Martens-Habbena W., Berube P. M., Urakawa H., De La Torre J. R. and Stahl D. A. (2009) Ammonia oxidation kinetics determine niche separation of nitrifying Archaea and Bacteria. *Nature* **461**, 976–979.

McFarlin J. M., Axford Y., Masterson A. L. and Osburn M. R. (2019) Calibration of modern sedimentary δ2H plant wax-water relationships in Greenland lakes. *Quat. Sci. Rev.* **225**, 105978.

Möller-Zinkhan D., Börner G. and Thauer R. K. (1989) Function of methanofuran, tetrahydromethanopterin, and coenzyme F42oin Archaeoglobusfulgidus.

Möller-Zinkhan D. and Thauer R. K. (1990) Anaerobic lactate oxidation to 3 CO2 by Archaeoglobus fulgidus via the carbon monoxide dehydrogenase pathway: demonstration of the acetyl-CoA carbon-carbon cleavage reaction in cell extracts. *Arch. Microbiol.* **153**, 215–218.

Morgan R. M., Pihl T. D., Lling J. R. N. and Reeve J. N. (1997) Hydrogen Regulation of Growth, Growth Yields, and Methane Gene Transcription in Methanobacterium thermoautotrophicum ⌬H. *J BACTERIOL* **179**.

Osburn M. R., Dawson K. S., Fogel M. L. and Sessions A. L. (2016) Fractionation of Hydrogen Isotopes by Sulfate- and Nitrate-Reducing Bacteria. *Front. Microbiol.* **7**.

Pearson A. (2014) Lipidomics for Geochemistry. In *Treatise on Geochemistry* Elsevier. pp. 291–336.

Pereira I. A. C., Ramos A. R., Grein F., Marques M. C., Da Silva S. M. and Venceslau S. S. (2011) A Comparative Genomic Analysis of Energy Metabolism in Sulfate Reducing Bacteria and Archaea. *Front. Microbiol.* **2**.

Reed D. W. and Hartzell P. L. (1999) The Archaeoglobus fulgidus D-Lactate Dehydrogenase Is a Zn2Ƨ Flavoprotein. *J BACTERIOL* **181**.

Rhim J. H., Zhou A., Amenabar M. J., Elling F. J., Weber Y., Pearson A., Boyd E. S. and Leavitt W. D. (2023) *Mode of carbon and energy metabolism shifts lipid composition in the thermoacidophile* Acidianus., Microbiology.

Rohmer M., Knani M., Simonin P., Sutter B. and Sahm H. (1993) Isoprenoid biosynthesis in bacteria: a novel pathway for the early steps leading to isopentenyl diphosphate. *Biochem. J.* **295**, 517–524.

Russell J. B. (2007) The Energy Spilling Reactions of Bacteria and Other Organisms. *Microb. Physiol.* **13**, 1–11.

Sachs J. P. (2014) Hydrogen Isotope Signatures in the Lipids of Phytoplankton. In *Treatise on Geochemistry* Elsevier. pp. 79–94.

Sachs J. P. and Kawka O. E. (2015) The Influence of Growth Rate on 2H/1H Fractionation in Continuous Cultures of the Coccolithophorid Emiliania huxleyi and the Diatom Thalassiosira pseudonana ed. G. P. Tochtrop. *PLOS ONE* **10**, e0141643.

Sachs J. P., Maloney A. E. and Gregersen J. (2017) Effect of light on 2H/1H fractionation in lipids from continuous cultures of the diatom Thalassiosira pseudonana. *Geochim. Cosmochim. Acta* **209**, 204–215.

Sachs J. P., Maloney A. E., Gregersen J. and Paschall C. (2016) Effect of salinity on 2H/1H fractionation in lipids from continuous cultures of the coccolithophorid Emiliania huxleyi. *Geochim. Cosmochim. Acta* **189**, 96–109.

Sachse D., Billault I., Bowen G. J., Chikaraishi Y., Dawson T. E., Feakins S. J., Freeman K. H., Magill C. R., McInerney F. A., van der Meer M. T. J., Polissar P., Robins R. J., Sachs J. P., Schmidt H.-L., Sessions A. L., White J. W. C., West J. B. and Kahmen A. (2012) Molecular Paleohydrology: Interpreting the Hydrogen-Isotopic Composition of Lipid Biomarkers from Photosynthesizing Organisms. *Annu. Rev. Earth Planet. Sci.* **40**, 221–249.

Schmitz R. A., Linder D., Stetter K. O. and Thauer R. K. (1991) N s,N1~ reductase (coenzyme F42o-dependent) and formylmethanofurandehydrogenase from the hyperthermophileArchaeoglobusfulgidus.

Schwender J., Seemann M., Lichtenthaler H. K. and Rohmer M. (1996) Biosynthesis of isoprenoids (carotenoids, sterols, prenyl side-chains of chlorophylls and plastoquinone) via a novel pyruvate/glyceraldehyde 3-phosphate non-mevalonate pathway in the green alga *Scenedesmus obliquus*. *Biochem. J.* **316**, 73–80.

Schwörer B., Breitung J., Klein A. R., Stetter K. O. and Thauer R. K. (1993) Formylmethanofuran: tetrahydromethanopterin formyltransferase and NS,N ~ dehydrogenase from the sulfate-reducing Archaeoglobusfulgidus: similarities with the enzymes from methanogenic Archaea.

Sessions A. L. (2016) Factors controlling the deuterium contents of sedimentary hydrocarbons. *Org. Geochem.* **96**, 43–64.

Sessions A. L., Burgoyne T. W., Schimmelmann A. and Hayes J. M. (1999) Fractionation of hydrogen isotopes in lipid biosynthesis. *Org. Geochem.* **30**, 1193–1200.

Sessions A. L., Jahnke L. L., Schimmelmann A. and Hayes J. M. (2002) Hydrogen isotope fractionation in lipids of the methane-oxidizing bacterium Methylococcus capsulatus. *Geochim. Cosmochim. Acta* **66**, 3955–3969.

Sessions A. L., Sylva S. P., Summons R. E. and Hayes J. M. (2004) Isotopic exchange of carbon-bound hydrogen over geologic timescales 1 1Associate editor: J. Horita. *Geochim. Cosmochim. Acta* **68**, 1545–1559.

Steinsbu B. O., Thorseth I. H., Nakagawa S., Inagaki F., Lever M. A., Engelen B., Ovreas L. and Pedersen R. B. (2010) Archaeoglobus sulfaticallidus sp. nov., a thermophilic and facultatively lithoautotrophic sulfate-reducer isolated from black rust exposed to hot ridge flank crustal fluids. *Int. J. Syst. Evol. Microbiol.* **60**, 2745–2752.

Stetter K. O. (1988) Archaeoglobus fulgidus gen. nov., sp. nov.: a New Taxon of Extremely Thermophilic Archaebacteria. *Syst. Appl. Microbiol.* **10**, 172–173.

Stouthamer A. H. and Bettenhaussen C. W. (1977) A continuous culture study of an ATPase-negative mutant of Escherichia coli. *Arch. Microbiol.* **113**, 185–189.

Thauer R. K., Kaster A.-K., Goenrich M., Schick M., Hiromoto T. and Shima S. (2010) Hydrogenases from Methanogenic Archaea, Nickel, a Novel Cofactor, and H_2 Storage. *Annu. Rev. Biochem.* **79**, 507–536.

Valentine D. L. (2007) Adaptations to energy stress dictate the ecology and evolution of the Archaea. *Nat. Rev. Microbiol.* **5**, 316–323.

Van Der Meer M. T. J., Benthien A., French K. L., Epping E., Zondervan I., Reichart G.-J., Bijma J., Sinninghe Damsté J. S. and Schouten S. (2015) Large effect of irradiance on hydrogen isotope fractionation of alkenones in Emiliania huxleyi. *Geochim. Cosmochim. Acta* **160**, 16–24.

Wakil S. J., Stoops J. K. and Joshi V. C. (1983) FATTY ACID SYNTHESIS AND ITS REGULATION.

Wijker R. S., Sessions A. L., Fuhrer T. and Phan M. (2019) $^{2}H/^{1}H$ variation in microbial lipids is controlled by NADPH metabolism. *Proc. Natl. Acad. Sci.* **116**, 12173–12182.

Wolfshorndl M., Danford R. and Sachs J. P. (2019) 2H/1H fractionation in microalgal lipids from the North Pacific Ocean: Growth rate and irradiance effects. *Geochim. Cosmochim. Acta* **246**, 317–338.

Wu W., Meador T. B., Könneke M., Elvert M., Wegener G. and Hinrichs K. (2020) Substrate-dependent incorporation of carbon and hydrogen for lipid biosynthesis by *Methanosarcina barkeri*. *Environ. Microbiol. Rep.* **12**, 555–567.

Zhang X., Gillespie A. L. and Sessions A. L. (2009) Large D/H variations in bacterial lipids reflect central metabolic pathways. *Proc. Natl. Acad. Sci.* **106**, 12580–12586.

Zhang Z. and Sachs J. P. (2007) Hydrogen isotope fractionation in freshwater algae: I. Variations among lipids and species. *Org. Geochem.* **38**, 582–608.